ornl

ORNL/CON-173

OAK RIDGE
NATIONAL
LABORATORY

MARTIN MARIETTA

Heat Pump Water Heater Laboratory Test and Design Model Validation

K. H. Zimmerman

OPERATED BY
MARTIN MARIETTA ENERGY SYSTEMS, INC.
FOR THE UNITED STATES
DEPARTMENT OF ENERGY

Printed in the United States of America. Available from
National Technical Information Service
U.S. Department of Commerce
5285 Port Royal Road, Springfield, Virginia 22161
NTIS price codes—Printed Copy: A06 Microfiche A01

This report was prepared as an account of work sponsored by an agency of the United States Government. Neither the United States Government nor any agency thereof, nor any of their employees, makes any warranty, express or implied, or assumes any legal liability or responsibility for the accuracy, completeness, or usefulness of any information, apparatus, product, or process disclosed, or represents that its use would not infringe privately owned rights. Reference herein to any specific commercial product, process, or service by trade name, trademark, manufacturer, or otherwise, does not necessarily constitute or imply its endorsement, recommendation, or favoring by the United States Government or any agency thereof. The views and opinions of authors expressed herein do not necessarily state or reflect those of the United States Government or any agency thereof.

ORNL/CON-173

Energy Division

HEAT PUMP WATER HEATER LABORATORY TEST AND DESIGN MODEL VALIDATION

K. H. Zimmerman

Date Published: March 1986

Prepared by the
OAK RIDGE NATIONAL LABORATORY
Oak Ridge, Tennessee 37831
operated by
MARTIN MARIETTA ENERGY SYSTEMS, INC.
for the
U.S. DEPARTMENT OF ENERGY
under Contract No. DE-AC05-84OR21400

CONTENTS

	Page
LIST OF FIGURES	v
LIST OF TABLES	vii
ACKNOWLEDGMENTS	ix
ABSTRACT	xi
SUMMARY	xiii
1. INTRODUCTION	1-1
2. EXPERIMENTAL FACILITY	2-1
2.1 Heat Pump Water Heater	2-1
2.1.1 Sensor Locations	2-2
2.2. Environmental Chamber	2-3
2.3 Data Acquisition System	2-5
2.4 Instrumentation	2-7
2.4.1 Pressure	2-7
2.4.2 Temperature	2-8
2.4.3 Flow rate	2-8
2.4.4 Power	2-8
2.4.5 Relative Humidity	2-8
2.4.6 Calibration	2-9
3. EXPERIMENTAL PROCEDURES	3-1
3.1 Recovery Tests	3-3
3.2 Steady-State Tests	3-3
3.3 Refrigerant Charge	3-3
3.4 Data Transfer Process	3-3
4. TEST RESULTS	4-1
4.1 Recovery Tests	4-1
4.1.1 Ambient Temperature Effect	4-1
4.2 Steady-State Tests	4-2
4.2.1 Measurement Reliability	4-2
4.2.2 Ambient Temperature Effect	4-4
4.2.3 HPWH Inlet Water Temperature Effect	4-12
4.2.4 Relative Humidity Effect	4-15
5. COMPUTER DESIGN MODEL	5-1
5.1 Model Modification	5-1
5.1.1 Water-to-Refrigerant Condenser Routine	5-1
5.1.2 Circulating Water Pump Routine	5-4
5.2 Model Validation	5-6
6. RECOMMENDATIONS	6-1

7. REFERENCES 7-1

Appendix A. EXPERIMENTAL DATA A-1

Appendix B. DESCRIPTION OF INPUT DATA FORMAT B-1

Appendix C. SAMPLE INPUT DATA C-1

Appendix D. SAMPLE OUTPUT D-1

Appendix E. LISTING OF CIRCULATING WATER PUMP ROUTINE E-1

LIST OF FIGURES

		Page
1.	Heat pump water heater test loop	2-1
2.	Closeup view of instrumented HPWH	2-2
3.	Air conditioning system refrigeration cycle	2-5
4.	Overall view of test site	2-6
5.	Data acquisition system	2-6
6.	Closeup view of DAS	2-7
7.	Recovery test flowchart	3-1
8.	Steady-state test flowchart	3-2
9.	Effect of ambient temperature on recovery efficiency	4-2
10.	Effect of ambient temperature on recovery rate	4-3
11.	Effect of ambient temperature on evaporator exit saturation temperature and pressure	4-6
12.	Effect of evaporator saturation temperature on refrigerant density	4-7
13.	Effect of ambient temprature on compressor work and compressor work per unit mass of refrigerant required	4-8
14.	Effect of ambient temprature on evaporator capacity	4-9
15.	Effect of ambient temperature on condenser capacity	4-9
16.	Effect of ambient tmperature on enthalpy change through the condenser	4-10
17.	Effect of ambient temperature on COP	4-11
18.	Effect of ambient temperature on compressor shell heat loss	4-11
19.	Effect of HPWH inlet water temperature on enthalpy change through condenser	4-13
20.	Effect of HPWH inlet water temperature on condenser capacity	4-14
21.	Effect of HPWH inlet water temperature on total power consumption	4-14

22. Effect of HPWH inlet water temperature on COP 4-15

23. Cross section of condenser tubes 5-2

24. Circulating water pump characteristic curves 5-5

25. Pump and system total head curves 5-5

LIST OF TABLES

		Page
1.	Heat pump water heater features	2-3
2.	Sensor locations	2-4
3.	Error analysis on heat balance	4-3
4.	Measurements used in heat balance	4-4
5.	Influence of ambient temperature on compressor efficiency	4-12
6.	Influence of inlet water temperature on compressor efficiency	4-15
7.	Influence of relative humidity on performance	4-16
8.	Tube-in-tube condenser dimensions	5-1
9.	Tube-in-tube condenser constants	5-3
10.	Comparison of measured values with compressor map model predictions	5-6
11.	Pump characteristics	5-7
12.	Heat pump water heater model validation at 21.2°C) (70.2°F) ambient 54.1% RH, and 52.6°C (126.6°F) entering water temperature	5-8
13.	Heat pump water heater model validation at 34.3°C (93.8°F) ambient, 60.7% RH, and 50.1°C (122.1°F) entering water temperature	5-9
14.	Heat pump water heater model validation at 10.6°C (51.0°F) ambient, 66% RH, and 46.9°C (116.4°F) entering water temperature	5-10
15.	Difference between the model calculated values (without and with the compressor map corrections) and the measured values at 10.6°C (51.0°F) ambient	5-10
A.1.	Performance data for steady-state tests run under various ambient conditions	A-2
A.2.	Performance data for a steady-state test run at various entering water temperatures	A-4

ACKNOWLEDGMENTS

The author would like to thank the following people for their contributions: (1) D. E. Holt for setting up the test site; (2) J. T. Farmer for maintenance of the refrigeration system; (3) W. W. Smith for the system's electrical wiring; (4) R. L. Linkous for running experiments; (5) S. K. Fischer and C. K. Rice for assistance with the computer design model; (6) T. J. Simmons for word processing of the report; (7) L. D. Gilliam for graphics in the reports; and (8) Mary Guy for editing the report.

ABSTRACT

A residential separated-type heat pump water heater (HPWH) unit was tested in a laboratory under controlled environmental conditions. Steady-state tests were conducted over a range of ambient temperatures, relative humidities, and inlet water temperatures. For the ambient temperature rise from 10 to 38°C (50 to 100°F), the evaporator capacity increased 62%, the condenser capacity increased 67%, and the coefficient of performance (COP) improved 34% (from 1.89 to 2.54). As the HPWH condenser inlet water temperature increased from 46 to 54°C (115 to 130°F) while the ambient temperature remained 23°C (73°F), the condenser capacity decreased 4% and the COP declined 14% (from 2.21 to 1.89). Test data were used to form a data base on HPWH performance which was subsequently used to validate the HPWH design model. The HPWH design model, a computer program derived from the existing ORNL Heat Pump Design Model, was proven to be capable of predicting the performance of the separated-type HPWH system and is intended to be used in studies concerning the improvement of HPWH performance.

SUMMARY

Heat pump water heater (HPWH) units were first built in the late 1950's, but only recently gained attention because of the rising cost of electricity. The HPWH units now available are first-generation design. They are assembled with available components that were developed for other uses. Therefore, it is likely that the performance of the units can be improved.

The objective of this project was to collect sufficient data from the experimental study to form a data base on the performance of a residential separated-type HPWH unit which would be subsequently used to formulate and validate an analytical steady-state design model.

The HPWH used in this study was representative of the residential separated-type units currently available on the market. It was connected to a water storage tank and fully instrumented to measure refrigerant and water temperatures, refrigerant pressures, refrigerant and water flow rates, and power consumptions of the components.

To obtain data of sufficient accuracy, the experimental facility was housed in an environmental chamber having controlled temperature and humidity. Steady-state tests were performed to study the effect of changing the ambient temperature, humidity, and entering water temperature on HPWH component and system performances. Data were collected using a digital voltmeter, a multiprogrammer, and a scanner controlled by a desktop computer.

The HPWH computer design model is a modification of the ORNL Heat Pump Design Model (HPDM). Necessary additions to the ORNL HPDM were a water-to-refrigerant condenser routine (developed at Brookhaven National Laboratory) and a water pump routine (developed at ORNL). To accomplish incorporation of these routines into the model, five new routines were added and eight routines were revised.

Data from several steady-state tests were input into the HPWH design model for validation purposes.

The recovery efficiency and recovery rate are values typically used in rating all types of water heaters. Initial tests were performed under a range of ambient temperatures. They showed the recovery efficiency increasing 61% from 1.79 to 2.89 as the ambient temperature rose from 10 to 38°C (50 to 100°F). The recovery rate increased 89% from 34.9 to 65.9 L/h (9.2 to 17.4 gal/h) as the ambient temperature changed from 10 to 38°C (50 to 100°F).

Steady-state HPWH tests were performed at ambient temperatures ranging from 10 to 38°C (50 to 100°F). As the ambient temperature increased, the results showed an increase in evaporator capacity of 62%, an increase in condenser capacity of 67%, and an increase in the coefficient of performance (COP) of 34% from 1.89 to 2.54.

During steady-state operation at a constant ambient temperature of 23°C (73°F), the condenser capacity decreased 4% and the COP declined 14% from 2.21 to 1.89 as the HPWH inlet water temperature increased from 46 to 54°C (115 to 130°F). As expected at higher relative humidity steady-state conditions, the evaporator capacity, condenser capacity, and COP increased.

The data base formed from the laboratory tests was used to validate the HPWH steady-state design model. Main differences between the experimentally measured and model calculated results were found to be in the pressure drop across the evaporator and the

compressor map predictions. When these inaccuracies were corrected, the model predicted the performance of the heat pump within 5% of the measured value. These validation runs proved the model to be capable of predicting the performance of a residential separated-type HPWH unit.

The next step in this project would be to use the HPWH design model in a parametric study followed by an optimization study. These studies would provide an analytical capability to evaluate the effect of improved components or new design features on the HPWH system performance.

1. INTRODUCTION

Heat pump water heater (HPWH) units were first built in the late 1950s, but only recently gained attention because of the rising cost of electricity. The HPWH units now available are first-generation design. They are assembled with available components that were developed for other uses. Therefore, it is likely that the performance of the units can be improved.

The objective of this experimental study was to collect sufficient data to form a data base on the performance of a residential HPWH unit. The data base was used to formulate and validate an analytical steady-state design model.

The experimental tests described in this report were conducted to study the effect of changing ambient temperature, humidity, and entering water temperatures on HPWH component and system performance. Primarily steady-state tests, but also recovery tests, were performed.

2. EXPERIMENTAL FACILITY

2.1 HEAT PUMP WATER HEATER

The HPWH used in this study was representative of the separated-type units currently available on the market. A schematic of the instrumented HPWH test loop is shown in Fig. 1 and displayed in a close-up view in Fig. 2. The superheated R-12 refrigerant vapor enters the rotary compressor where it is compressed to a higher temperature and higher pressure vapor. The hot vapor passes through the annulus of the coaxial condenser where it surrenders its heat to the water which is simultaneously flowing countercurrent to the refrigerant through the inner tube of the condenser. Warmed water is then pumped to the

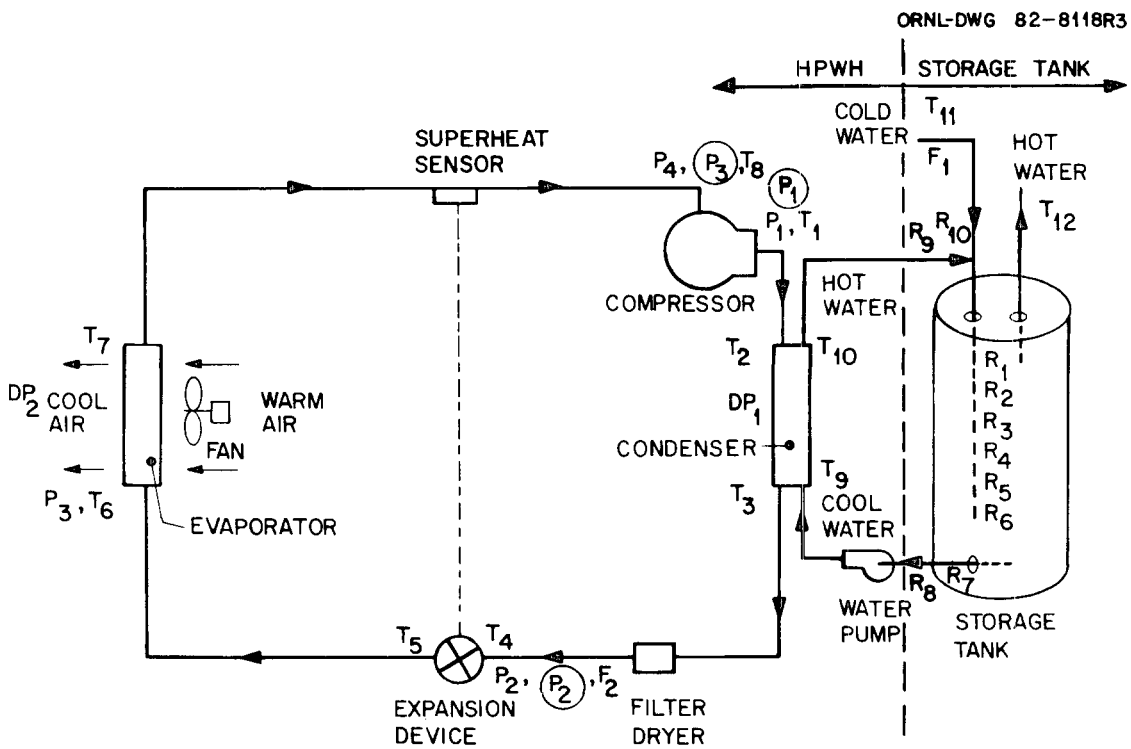

T_{1-12} — THERMOCOUPLES

R_{1-10} — RTDs

P_{1-4} — ABSOLUTE PRESSURE TRANSMITTERS

DP_{1-2} — DIFFERENTIAL PRESSURE TRANSMITTERS

P_{1-3} — PRESSURE GAGES

F_{1-3} — FLOWMETERS

HPWH — HEAT PUMP WATER HEATER

Fig. 1. Heat pump water heater test loop.

ORNL-PHOTO 6783-83

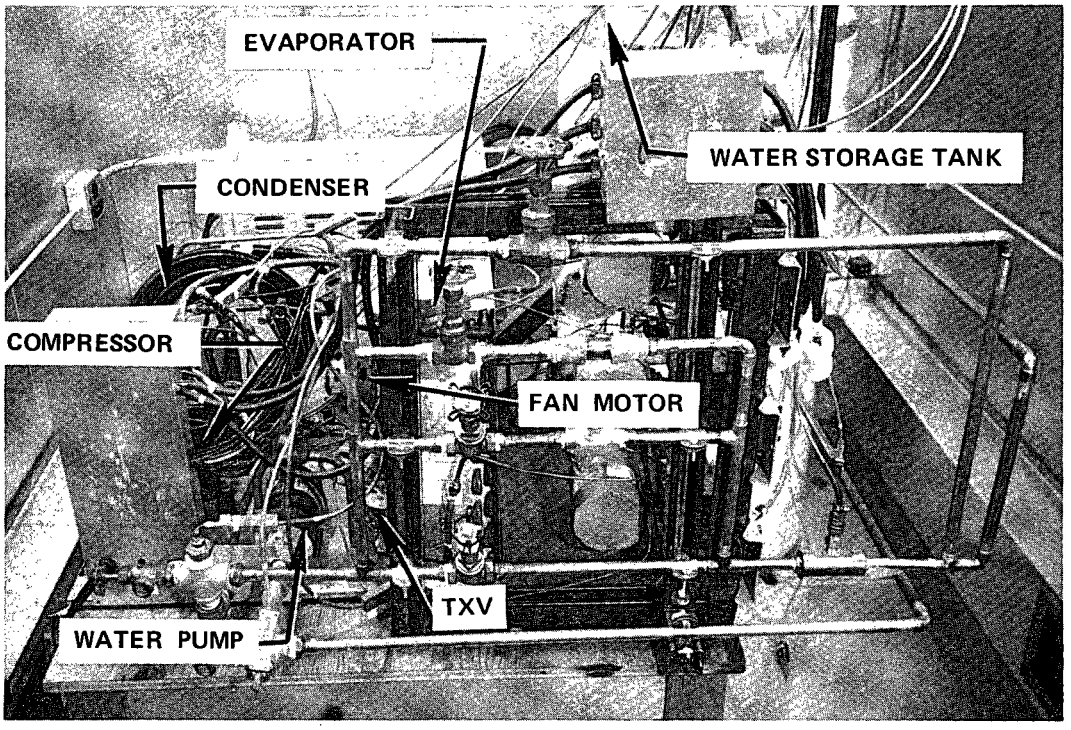

Fig. 2. Closeup view of instrumented HPWH.

water storage tank by the water circulating pump. Warm, condensed liquid refrigerant is throttled by the thermostatic expansion valve (TXV) to a lower pressure and temperature and becomes a liquid/vapor mixture. The TXV continuously monitors the evaporator exit superheat and adjusts the refrigerant feed rate to maintain the superheat at a constant level. The cold refrigerant mixture then flows through the evaporator tubes as the room air is blown across the finned tubes by the fan, thus evaporating the liquid refrigerant. Cool refrigerant vapor leaves the evaporator and returns to the compressor, completing the cycle. A detailed description of the HPWH is found in Table 1.

The HPWH unit was connected to a 311-L (82-gal) storage tank with copper tubing insulated to prevent recirculation of the water due to natural thermal convection. A closed water loop is formed by the HPWH, the water tubing, the water storage tank, and the water circulating pump. Water is pumped by the circulating pump from the bottom of the storage tank, through the condenser where it picks up heat, to the top of the storage tank. There it enters a dip tube installed in the storage tank and flows down approximately two-thirds of the length of the tank and exits into the bottom portion of the tank.

2.1.1 Sensor Locations

Temperature, pressure, and flow-rate readings were measured on the HPWH refrigerant and water circuits at the locations shown in Fig. 1. Table 2 describes the corresponding

Table 1. Heat pump water heater features

Refrigerant R-12
1.3-cm (0.5-in.) outside diameter (OD) copper water tubing
0.95-cm (0.375-in.) discharge, 1.3-cm (0.5-in.) suction OD copper refrigerant tubing

COMPRESSOR

- rotary
- accumulator on suction line
- 23.4-cm^3 (1.43-$in.^3$) displacement
- 3.0 kW (10,200 Btu/h) rated for R-12 at
  - 54.4°C (130°F) condensing temperature
  - 7.2°C (45°F) evaporating temperature
  - 35°C (95°F) ambient temperature

EVAPORATOR

- 2 tubes deep
- 16 tubes high
- 0.8-cm (0.13-in.) OD copper tubing
- 11 wavy aluminum fins per 2.54 cm (1.0 in.)
- 0.17-m^2 (1.78-ft^2) frontal area

CONDENSER

- horizontal coil axis
- 4.9-m (10-ft.) total tube length
- tube-in-tube construction
- 2.54-cm (1.0-in) OD refrigerant tube
- 1.4-cm (0.56-in.) OD water tube
- counterflow type
- insulated
- 4.4-kW (1.25-ton) nominal rating

EVAPORATOR FAN

- 0.24-m^3/s (500-cfm) air flow
- 1575 rpm
- 1.5 amps

EXPANSION DEVICE

- thermostatic
- 2.6 kW (0.75 ton)

WATER PUMP

- magnetic drive
- 63 W maximum

location of the sensors numbered in Fig. 1. Power input to the compressor, fan motor, and the water pump was measured with watt/watthour transducers.

2.2 ENVIRONMENTAL CHAMBER

To obtain data of sufficient accuracy from the experiment, it was necessary to house the experimental facility in an environmental chamber having controlled temperatures and humidity. A modular temperature/humidity conditioning system was attached to a 14.5-m^3 (512-ft^3) insulated chamber with 20.3-cm-diam (8-in.) flexible insulated hoses. Approximately 0.24 m^3/s (500 cfm) of conditioned air circulates from the air supply discharge through a flexible hose to the top of the chamber. The air then spreads out through a diffuser down into the chamber. The air flows through grates and into ducting installed on the lower inside perimeter of the chamber walls. The air exits the chamber through a flexible hose and returns to the air supply inlet to complete its cycle. The refrigeration system for the air conditioning system is shown schematically in Fig. 3. The air conditioning system and insulated chamber are represented in an overall view in Fig. 4.

During the HPWH experiments, the air supply system controlled air temperatures in the chamber at various levels between 7 and 38°C (45 and 100°F) and relative humidities between 25 and 70%.

The temperature controller utilized in the air supply system is an electronic, solid-state instrument with proportional band, automatic reset, and rate control. Air temperature is

Table 2. Sensor locations

Sensor	Circuit[a]	Location
T_1	R	Compressor discharge
T_2	R	Condenser inlet
T_3	R	Condenser exit
T_4	R	Thermostatic expansion device inlet
T_5	R	Thermostatic expansion device exit
T_6	R	Evaporator inlet
T_7	R	Evaporator exit
T_8	R	Compressor suction
T_9	W	Condenser inlet
T_{10}	W	Condenser exit
T_{11}	W	Supply to water storage tank
T_{12}	W	Delivery from water storage tank
R_1	W	Water storage tank centerline, 11 in. from top
R_2	W	Water storage tank centerline, 17 in. from top
R_3	W	Water storage tank centerline, 23 in. from top
R_4	W	Water storage tank centerline, 29 in. from top
R_5	W	Water storage tank centerline, 35 in. from top
R_6	W	Water storage tank centerline, 41 in. from top
R_7	W	Water storage tank exit
R_8	W	HPWH inlet
R_9	W	HPWH exit
R_{10}	W	Water storage tank inlet
F_1	W	Supply water storage tank
F_2	R	Condenser exit
F_3	W	HPWH exit
P_1	R	Compressor discharge
P_2	R	TXV inlet
P_3	R	Evaporator inlet
P_4	R	Compressor suction
DP_1	R	Across the condenser
DP_2	R	Across the evaporator
(P_1)	R	Compressor discharge
(P_2)	R	TXV inlet
(P_3)	R	Compressor suction

[a]R—refrigerant; W—water.

sensed by a platinum resistance temperature detector (RTD) located in the air circulation plenum at the blower discharge. Cooling capacity is modulated by opening and closing the hot gas bypass valve and liquid desuperheating expansion valve. The hot gas bypass valve bypasses hot discharge gas back to the compressor suction as the desuperheating expansion valve cools the hot gas by throttling liquid refrigerant mix with the warm refrigerant vapor in the suction line. The heating capacity is modulated by the controller energizing and de-energizing the resistance heaters.

The relative humidity controller operates in the same manner as the temperature controller. A wet and dry bulb technique of measuring humidity consisting of a type "E" thermocouple (for wet bulb temperature) and modulation of a thermistor (for dry bulb temperature) is utilized. Relative humidity is controlled by opening and closing the solenoid

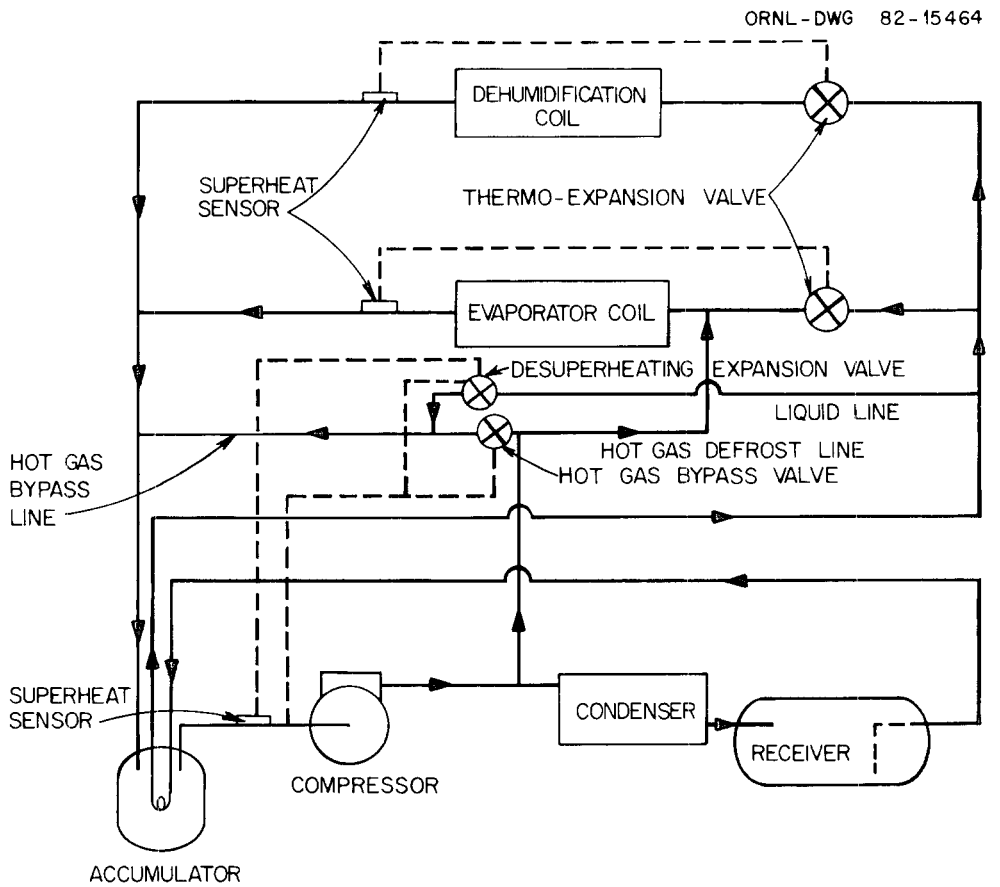

Fig. 3. Air conditioning system refrigeration cycle.

valve that controls the dehumidification coil (an additional evaporator coil that supplies latent cooling) and by bypassing a regulating thermostat. When the thermostat is bypassed, water boils in the steam generator and drives vapor into the chamber. Additional humidity was supplied by the building steam line, injecting steam into the chamber with on/off control from a hand valve.

2.3 DATA ACQUISITION SYSTEM

The data acquisition system (DAS) consists of a Hewlett Packard (HP) desktop computer, an HP digital voltmeter, an HP multiprogrammer, an HP multiprogrammer interface, an HP digital clock, an HP printer, and a Fluke scanner. A schematic of the DAS is shown in Fig. 5, and a closeup view is shown in Fig. 6. The desktop computer is configured with 62K bytes of memory and uses standard 9825 high-speed programming language (HPL). Voltage data signals are read from the instrumentation by the digital voltmeter. The multiprogrammer is the master control unit for input/output cards that perform such functions as closing relays to energize components and totalizing counts and contact closures from instrumentation. Bidirectional communication between the multiprogrammer and the computer is permitted by the multiprogrammer interface. The clock is a fully programmable

ORNL-PHOTO 6784-83

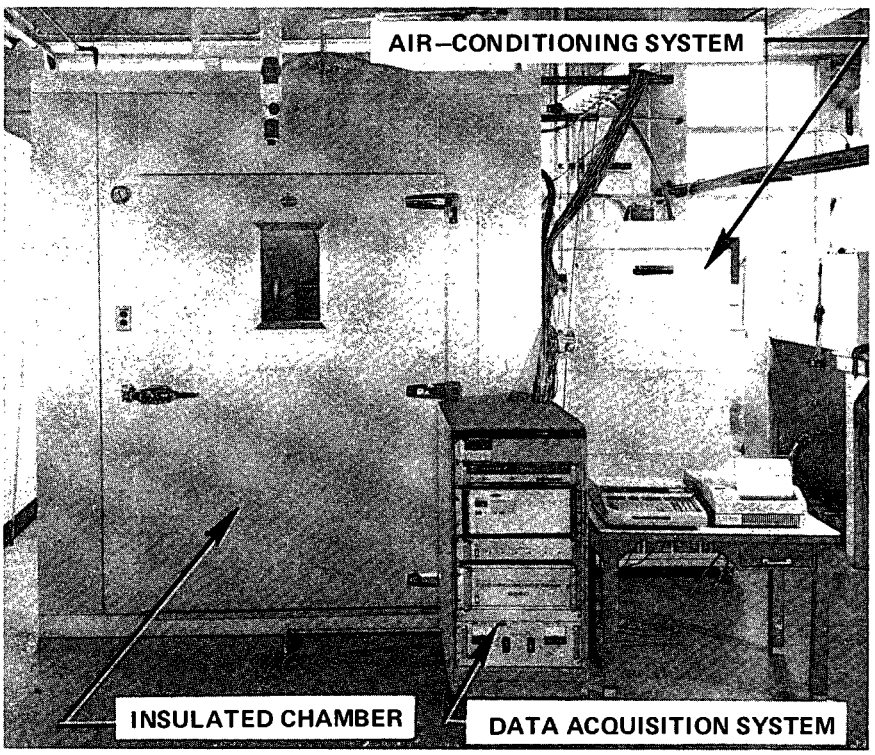

Fig. 4. Overall view of test site.

ORNL-DWG 84-7357

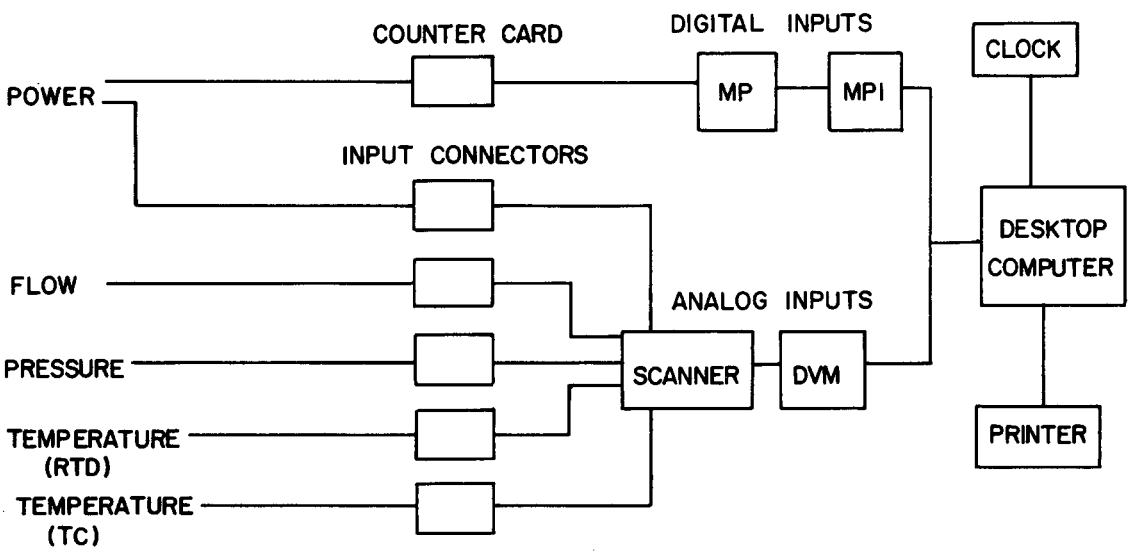

MP – MULTIPROGRAMMER
MPI – MULTIPROGRAMMER INTERFACE
DVM – DIGITAL VOLTMETER

Fig. 5. Data acquisition system.

ORNL-PHOTO 6811-83

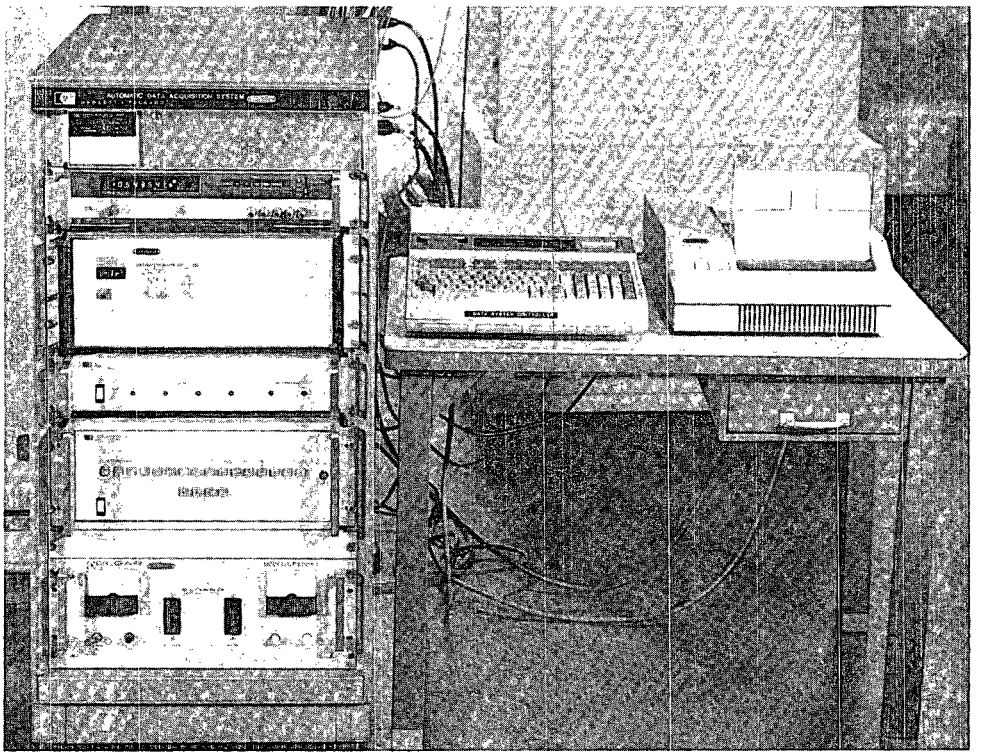

Fig. 6. Closeup view of DAS.

system calendar and time-of-day source and also serves as a stand-alone digital clock. The scanner is a channel selector that houses input connectors for analog data collection. Some descriptions of the input connectors and their functions are: (1) an isothermal block connector for thermocouple reference junction and measuring junction, (2) a current transmitter to convert current to voltage, and (3) an RTD connector to convert resistance to voltage.

2.4 INSTRUMENTATION

2.4.1 Pressure

The deflection of an internal diaphragm in the absolute and differential pressure transmitters was converted electronically to an amperage signal directly proportional to the pressure measured. A current transmitter connector installed in the scanner accepted the dc output current from the pressure transmitter and converted the current to a proportional dc voltage signal using precision shunt resistors. This signal was converted into pounds per square inch (psi) using a linear equation derived from calibration data. Bourdon-tube pressure gauges were manually read to check certain pressure transmitters.

2.4.2 Temperature

Thermocouples (TCs) and RTDs were installed on the system for measuring temperature. The RTDs were used where greater accuracy was demanded, such as for measuring a temperature difference. Two- and three-wire nickel-iron RTDs were mounted in stainless steel sheaths with copper lead wires producing a resistance signal. An input connector installed in the scanner supplied an adjustable current to the selected RTD. The resultant I-R drop was measured as a voltage. This voltage was converted to temperature in the software using a linear equation derived from calibration data. The copper-constantan TCs were attached to the outer surface of the refrigerant and water lines and covered with foam insulation to reduce temperature gradients through the tube wall. The measuring junction and floating reference junction located on the isothermal input connector produced voltage signals. National Bureau of Standard (NBS) tables were used to form fourth-order polynomial equations in the data collection software to convert from these signals to degrees Fahrenheit.

2.4.3 Flow Rate

Rotation of the propeller caused by fluid flow through the turbine flowmeters was sensed by an externally mounted pickoff as a train of electric pulses. The frequency of the pulses, which were directly proportional to the volume flow rate, was fed directly into a pulse to dc converter, and the resultant voltage signal was converted into gallons per minute in the software by using a linear equation derived from calibration data. Bypass lines were installed around the flowmeters to prevent damage by overspeeding the rotor on system start-up.

2.4.4 Power

The watt/watthour transducers provided two outputs simultaneously—an analog signal (current) directly proportional to instantaneous watts and a digital signal (frequency) directly proportional to watthours. The analog signal was converted to a proportional dc voltage, using precision shunt resistors that were located in the current transmitter connector installed in the scanner. A linear equation derived from calibration data was programmed in the data collection software to convert from voltage signal to watts. The digital signal was totalized by a pulse counter card installed in the multiprogrammer and similarly converted to watthours. Watthour meters were manually read to check the watt/watthour transducers.

2.4.5 Relative Humidity

Humidity was measured by using the wet bulb and dry bulb TC techniques. The wet bulb TC was enclosed in a wick, a portion of which was immersed in a container storing distilled water. The dry bulb TC was located next to the wet bulb. A fan was used to provide proper air velocity across the wet bulb. Wet bulb and dry bulb temperature readings were converted to relative humidity using psychrometric routines.

2.4.6 Calibration

All instruments were calibrated so that comparison of the tested instrument against a known standard could be made and thus reduce errors in accuracy. All calibrations, except for the flowmeters, were performed by ORNL personnel.

1. The absolute pressure transmitters and gauges were calibrated using a standard dead-weight tester.
2. The differential pressure transmitters were compared to a standard water manometer.
3. The TCs were calibrated using an ice bath procedure, and the readings were compared to a standard precision thermometer.
4. The RTDs were compared to a standard platinum resistance thermometer.
5. The flowmeters were calibrated by the manufacturer using a standard flow-measurement facility.
6. The watt/watthour transducers were calibrated in a setup consisting of (a) an input wattage signal derived from a known current passing through a known resistor bank and (b) a precision counter totalizing the pulses.
7. The watthour meters were calibrated at ORNL by comparing the operation of the tested meter with a rotating standard meter.

The accuracy of all the standard instruments used in the calibrations is traceable to NBS.

3. EXPERIMENTAL PROCEDURE

Experimental tests were conducted to study the effect of changing the ambient temperature and humidity and the entering water temperature on the HPWH system performance. Ambient temperature was varied from 10 to 38°C (50 to 100°F), relative humidity from 28 to 97%, and entering water temperature from 46 to 54°C (115 to 130°F).

The test procedures were controlled by the DAS. Flow charts describing the procedures are shown in Figs. 7 and 8.

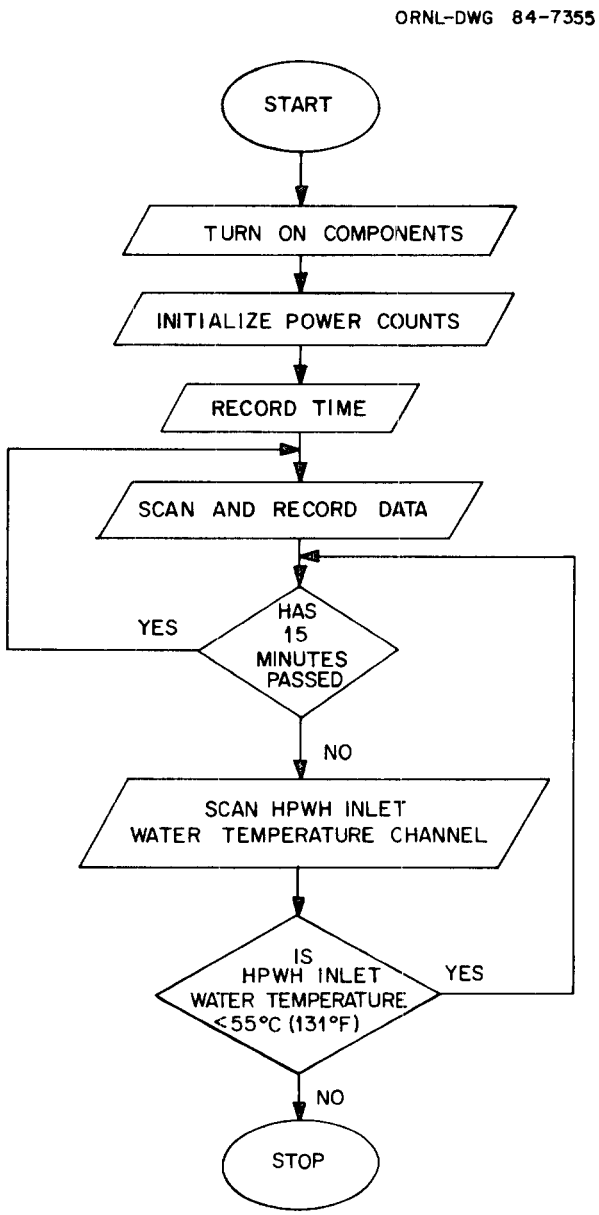

Fig. 7. Recovery test flowchart.

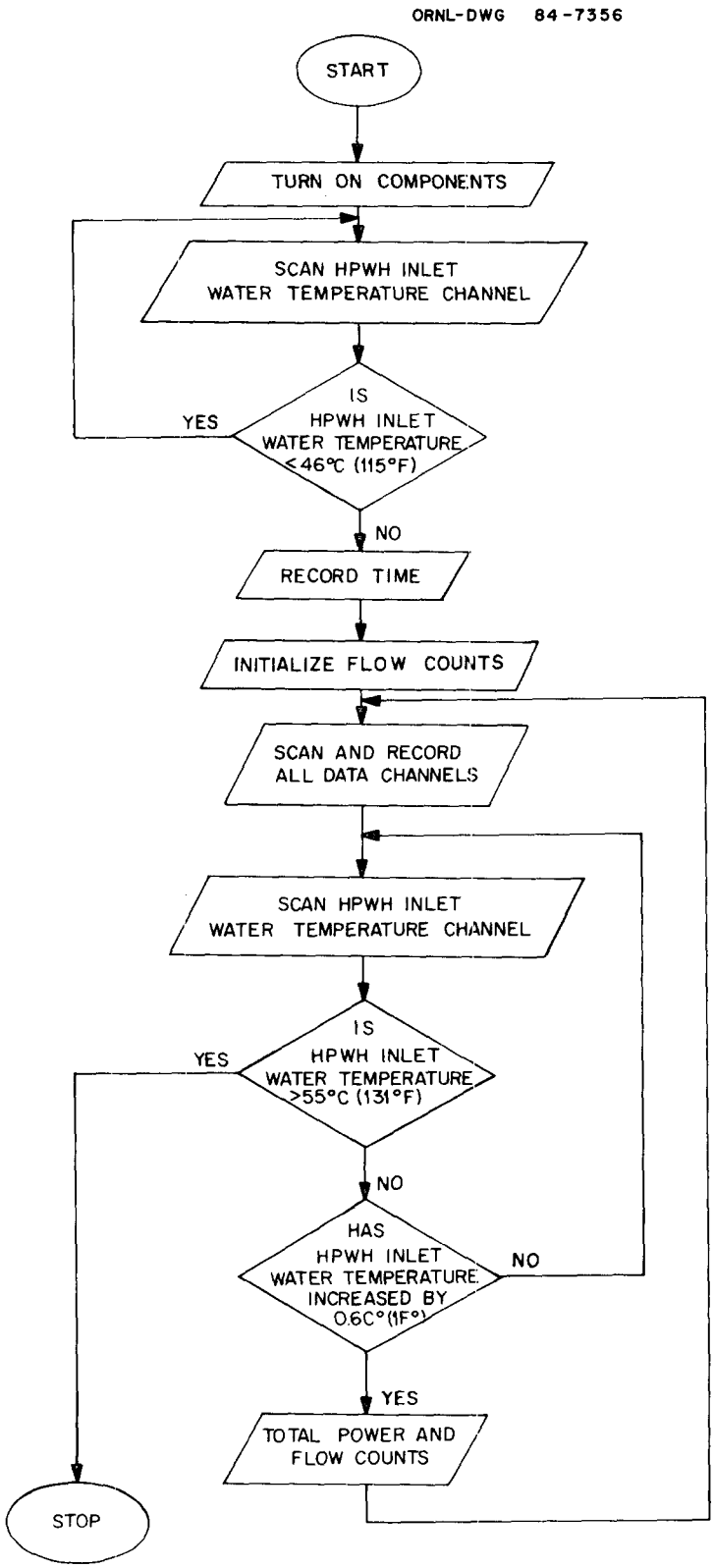

Fig. 8. Steady-state test flowchart.

3.1 RECOVERY TESTS

A recovery test began at start-up of the HPWH unit (compressor, fan motor, circulating water pump energized) with the supply water temperature at approximately 13°C (55°F) and continued until the HPWH inlet water temperature reached 55°C (131°F). At this time the HPWH unit was turned off. Data were collected every 15 min.

3.2 STEADY-STATE TESTS

A steady-state test began when the HPWH condenser inlet water temperature reached 46°C (115°F). By this time, the HPWH unit had been operating approximately 4 h. The entering water temperature was changing slowly enough [(0.6C° (1F°) per 3 to 5 min] to assume quasi-steady-state conditions.

Data were collected at every 0.6C° (1F°) rise of the HPWH inlet water temperature. The compressor, evaporator fan, and circulating water pump were operating for the entire duration of the test. The water was continuously circulated around the closed loop between the water storage tank and HPWH unit at a constant rate of 8.8×10^{-2} L/s (1.4 gpm). The test continued until the condenser inlet water temperature reached 55°C (131°F), at which time the HPWH was turned off.

The water temperature range of 46 to 55°C (115 to 131°F) was chosen to represent steady-state conditions. This temperature range is the typical on and off points of the HPWH unit when in normal "as installed by the dealer" operation.

3.3 REFRIGERANT CHARGE

The HPWH unit was charged to match the manufacturer's recommended value of suction pressure and discharge pressure when operated at a specific ambient temperature. This process resulted in a total charge of 1.1 kg (2.5 lb) of refrigerant, which was 0.4 kg (14 oz) over the nameplate charge of 0.7 kg (26 oz). The additional amount was needed to fill the copper tubing added to the system for installation of the pressure transmitters and refrigerant flowmeter.

3.4 DATA TRANSFER PROCESS

The raw data were collected by the HP desktop computer and stored on HP cassette tapes. Data were transferred to the ORNL main computer system via terminal emulator software and stored in files on disk storage space for reduction and analysis.

4. TEST RESULTS

4.1 RECOVERY TESTS

4.1.1 Ambient Temperature Effect

The recovery efficiency and recovery rate are values typically used in rating all types of water heaters. The recovery efficiency (E_r) given in Eq. 1 (ref. 1) is defined as the ratio of the heat imparted to the water to the energy input to the heat source. The tank losses are not taken into account.

$$E_r = \frac{K\,V\,\Delta T_1}{Z} \quad , \tag{1}$$

where

K = 1.15 Wh/L °C (8.25 Btu/gal °F), the nominal specific heat of water;

V = tank capacity [L (gal)];

ΔT_1 = difference between initial and final mean tank temperature in water storage tank, expressed in °C (°F);

Z = total electrical power input to HPWH components, expressed in Wh (Btu).

The recovery efficiency as a function of ambient temperature is shown in Fig. 9. The efficiency increases 61% from 1.79 to 2.89 as the ambient temperature rises from 10 to 38°C (50 to 100°F).

The recovery rate given in Eq. 2 (ref. 1) is defined as the rate in liters per hour (gallons per hour) of water that the HPWH is capable of heating normalized to a temperature rise of 50C° (90F°).

$$R = \frac{V\,\Delta T_1}{t\,\Delta T_2} \quad , \tag{2}$$

where

V and ΔT_1 are previously defined;

t = duration of recovery test, expressed in hours;

ΔT_2 = 50C° (90F°).

The recovery rate as a function of ambient temperature is shown in Fig. 10. The recovery rate increases 89% from 34.9 to 65.9 L/h (9.2 to 17.4 gal/h) as the ambient temperature changes from 10 to 38°C (50 to 100°F).

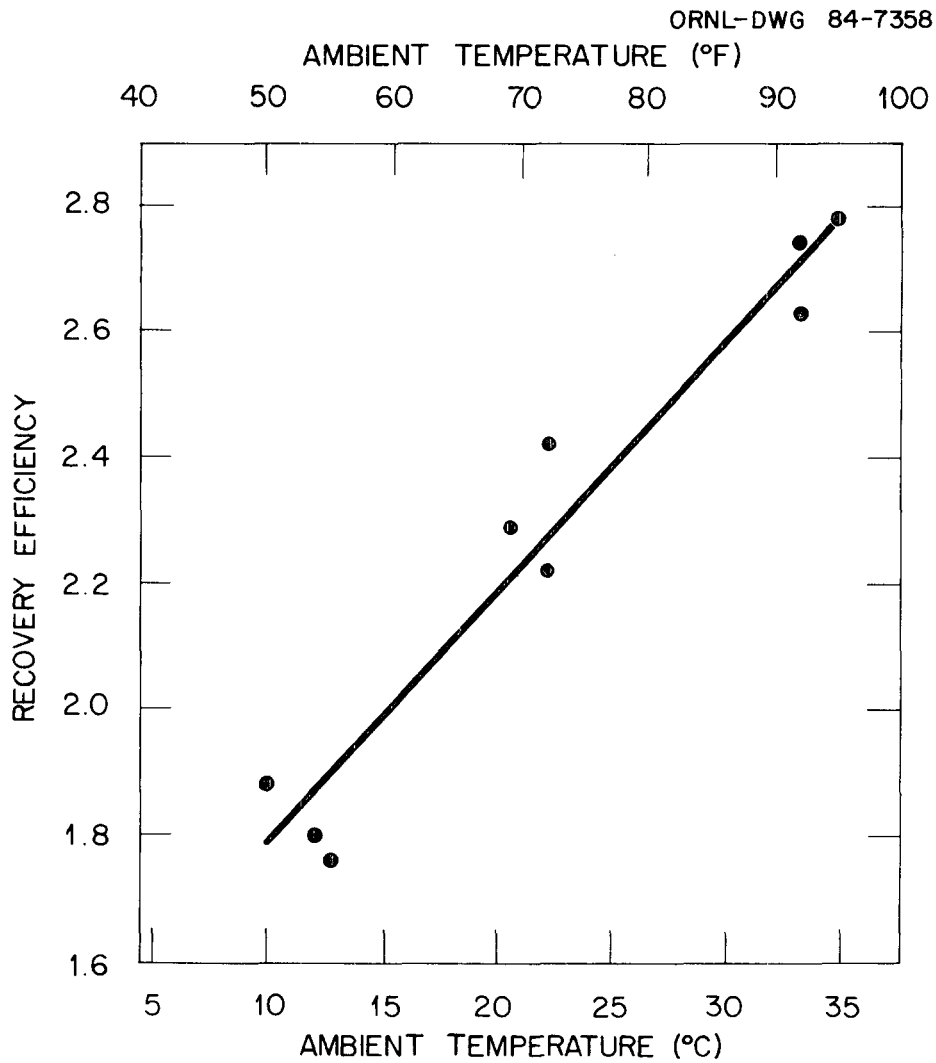

Fig. 9. Effect of ambient temperature on recovery efficiency.

4.2 STEADY-STATE TESTS

4.2.1 Measurement Reliability

The condenser heat balance of the refrigerant-side compared to the water-side was rarely in agreement. An error analysis was made on the heat balance by calculating the effect of an error in a data point measurement on the capacity. The results are tabulated in Table 3.

As is shown in Table 3, the water temperature has the greatest influence on capacity. The water temperatures were being measured using a thermocouple (TC) strapped to the outside of the water tube and covered with insulation. To provide a more accurate measurement, the TC was removed from the pipe and immersed in a well installed in the pipe. The TC now read closer to the actual water stream temperature. However, this new method did not correct the heat balance error.

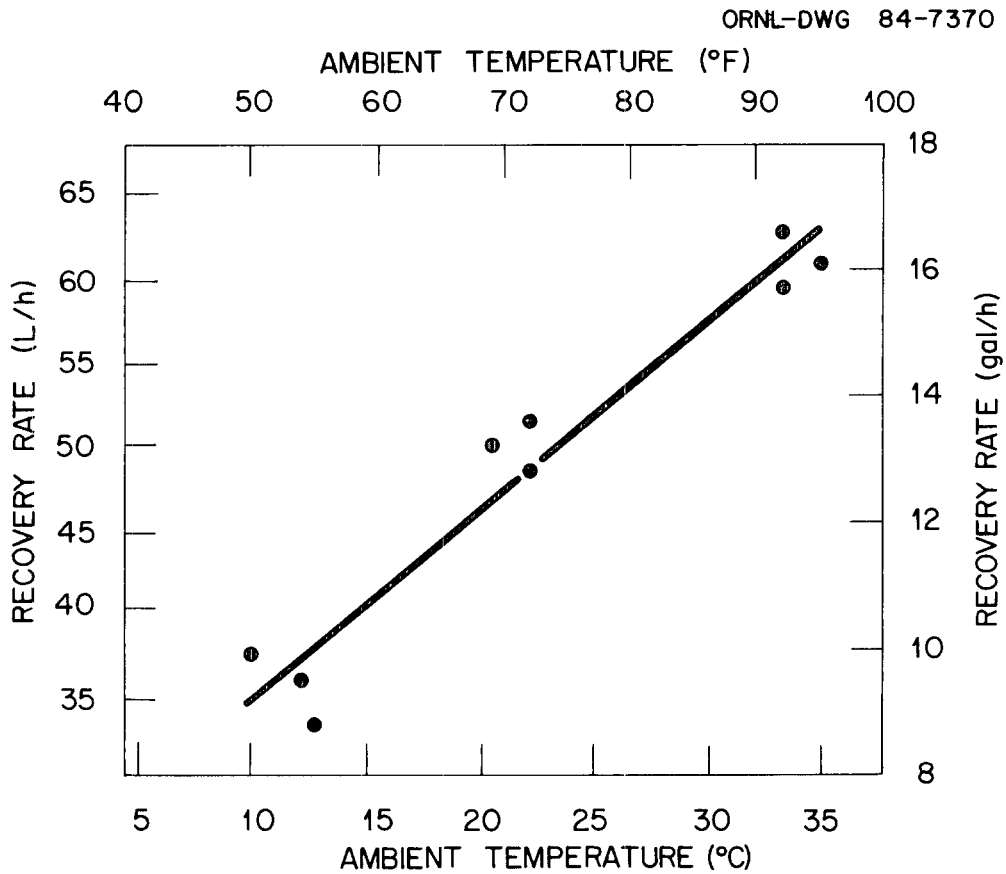

Fig. 10. Effect of ambient temperature on recovery rate.

Table 3. Error analysis on heat balance

Measured values	Change of values	Change in capacity
Water temperature, C° (F°)	0.6 (1.0) 0.8%	9.0%
Water flow rate, L/s (gpm)	0.006 (0.1) 7.3%	7.3%
Refrigerant flow rate, L/s (gpm)	0.0006 (0.01) 3.7%	3.7%
Refrigerant temperature, °C (°F)	0.6 (1.0) 0.7%	<1.0%

The water flow rate had the next greatest effect on capacity. The flowmeter was recalibrated by opening the water loop and running the water through the flowmeter and into a bucket located on a platform scale. The weight and duration of the calibration was used to calculate the flow rate. The calculated reading compared closely to the flowmeter reading. Again, this was not the cause of the heat balance error.

The refrigerant flowmeter was sent to ORNL Instrumentation and Controls Division personnel for recalibration. Some epoxy particles were found in the flowmeter possibly

clogging the orifice or not allowing the turbine blades to spin properly. The flowmeter was cleaned up, recalibrated, and returned. More tests followed only to find the heat balances still in error. The electronics part of the flowmeter was checked out by switching the pickoff coil and pulse rate counter from the properly operating water flowmeter to the refrigerant flowmeter. The refrigerant flow rate reading did not change.

Although the refrigerant temperatures had a very small effect on capacity, they were compared to readings from a digital temperature probe. The measurements were in good agreement.

In preliminary tests and one actual test, the heat balance did agree within 10%. The measured values for the actual test were compared to the measured values of a test in which the heat balance was within 25% error. Both tests were run at the same ambient conditions. Table 4 compares the measured values. As is shown, the refrigerant flow rate has the greatest difference at 19% while the other measurements are within acceptable agreement.

For some unexplained reason, the refrigerant flowmeter did not operate properly in the system. Due to the confidence of all the other measurements used in the heat balance, the tests were continued and the refrigerant flow rate value used in calculations was derived from the condenser heat balance.

Table 4. Measurements used in heat balance

	Test A	Test B	Percent difference
Heat balance error, %	5	24	
Refrigerant flow rate, L/s (gpm)	0.013 (0.21)	0.011 (0.17)	19
Condenser water flow rate, L/s (gpm)	0.086 (1.37)	0.086 (1.37)	0
Condenser inlet refrigerant temperature, °C (°F)	85 (185)	82 (179)	3
Condenser exit refrigerant temperature, °C (°F)	50 (122)	52 (125)	2
Condenser inlet water temperature, °C (°F)	47 (117)	47 (117)	0
Condenser exit water temperature, °C (°F)	54 (129)	54 (130)	1

4.2.2 Ambient Temperature Effect

The graphs described in this section are the results of the experimental tests run with a HPWH inlet water temperature of 48.3°C (119°F), ambient temperatures ranging from 50 to 100°F, and relative humidities ranging from 28 to 97%. The effect of relative humidity on the HPWH performance will be discussed later in this report. Some of the raw data is presented in Table A.1 of Appendix A.

The ambient temperature is the major temperature driving force in the evaporator. As the ambient temperature increases from 10 to 38°C (50 to 100°F), the evaporator saturation

temperature increases from −1.4 to 15.8°C (29.4 to 60.4°F) and the evaporator exit pressure increases from 290 to 496 kPa (42 to 72 psia) as shown in Fig. 11. These increases cause the compressor inlet refrigerant vapor density to increase. The density of the saturated refrigerant vapor as a function of evaporator saturation temperature is shown in Fig. 12. The density increases 0.32 kg/m^3 (0.02 lb/ft^3) for every 0.6C° (1F°) saturation temperature rise.

The refrigerant mass flow rate ($\dot{m}_r$) is related to the density by Eq. 3 (ref. 2).

$$\dot{m}_r = \rho D S \eta_{\text{vol}} \ , \tag{3}$$

where

ρ = refrigerant vapor density,

D = total compressor displacement,

S = compressor motor speed,

η_{vol} = overall volumetric efficiency.

The displacement and rated motor speed are constant. The overall volumetric efficiency is only mildly dependent on ambient temperatures, as will be shown later. Therefore, from Eq. 3, as the density increases at higher ambient temperatures the mass flow rate goes up proportionally. Although higher mass flow rates require more compressor work, the compressor work required per unit mass decreases. As shown in Fig. 13 as the ambient temperature changes from 10 to 38°C (50 to 100°F), the required compressor work increases 27%, but the required compressor work per unit mass decreases 28%.

The evaporator capacity is defined as the heat energy transferred from the air to the refrigerant in the evaporator. This term does not include the power input to the evaporator fan motor which warms the air before it passes over the evaporator coil. As shown in Fig. 14 as the ambient temperature changes from 10 to 38°C (50 to 100°F), the evaporator capacity increases 62%.

The heat rejected from the condenser into the water storage tank is basically a sum of the increased evaporator capacity and increased power input to the compressor. From these combined effects the heat rejected from the condenser (condenser capacity) increases 67% for the 10 to 38°C (50 to 100°F) ambient temperature change as shown in Fig. 15.

The coefficient of performance (COP) for HPWH units is defined as the ratio of the condenser capacity to the total power consumption.[3] This can be written as Eq. 4.

$$\text{COP} = \frac{\dot{Q}_{cond}}{\dot{W}_{\text{comp}} + \dot{W}_{\text{fan}} + \dot{W}_{\text{pump}}} \ , \tag{4}$$

where

$\dot{Q}_{\text{cond}}$ = condenser capacity,

$\dot{W}_{\text{comp}}$ = compressor power,

$\dot{W}_{\text{fan}}$ = fan motor power,

$\dot{W}_{\text{pump}}$ = pump power.

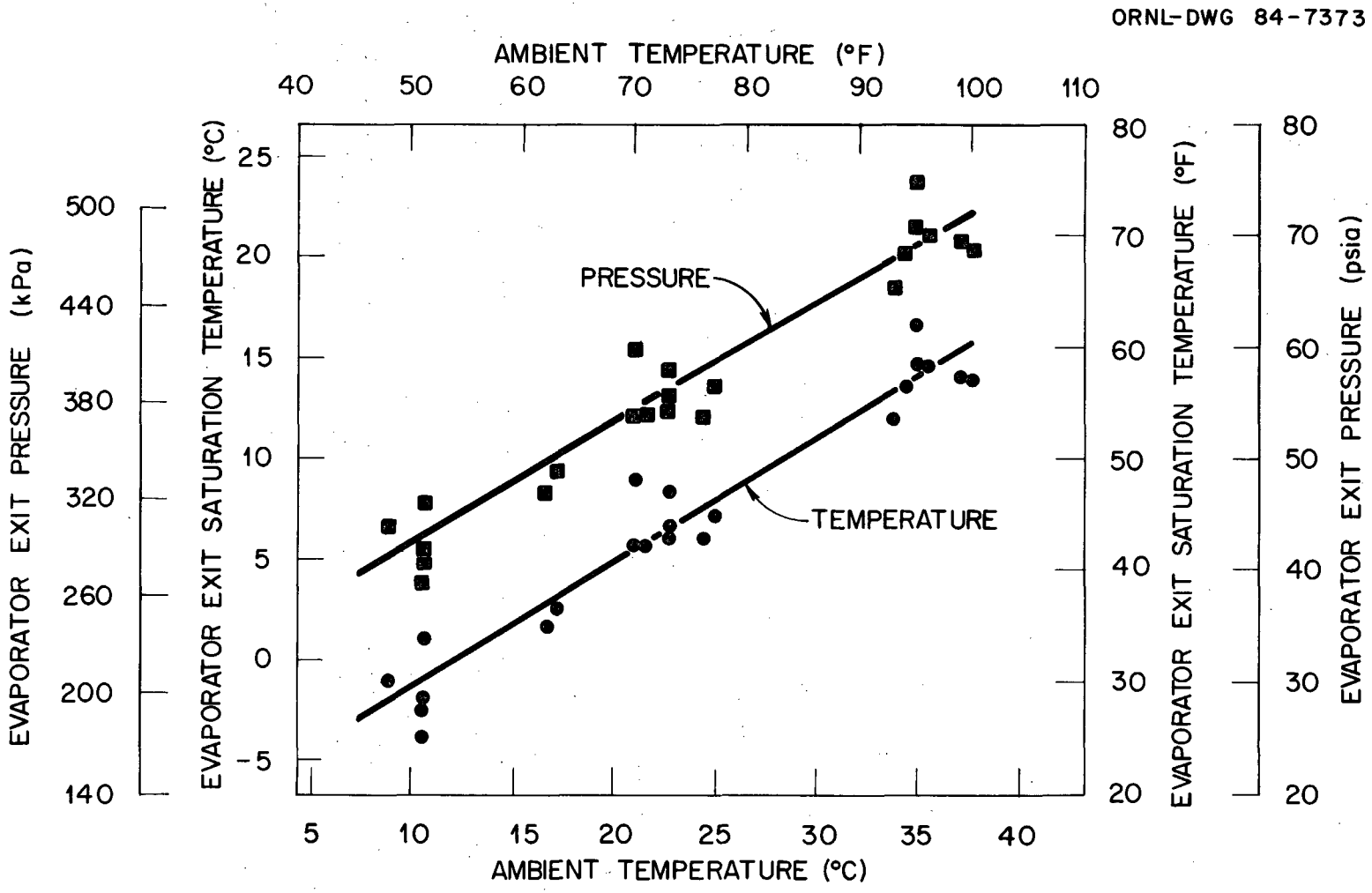

Fig. 11. Effect of ambient temperature on evaporator exit saturation temperature and pressure.

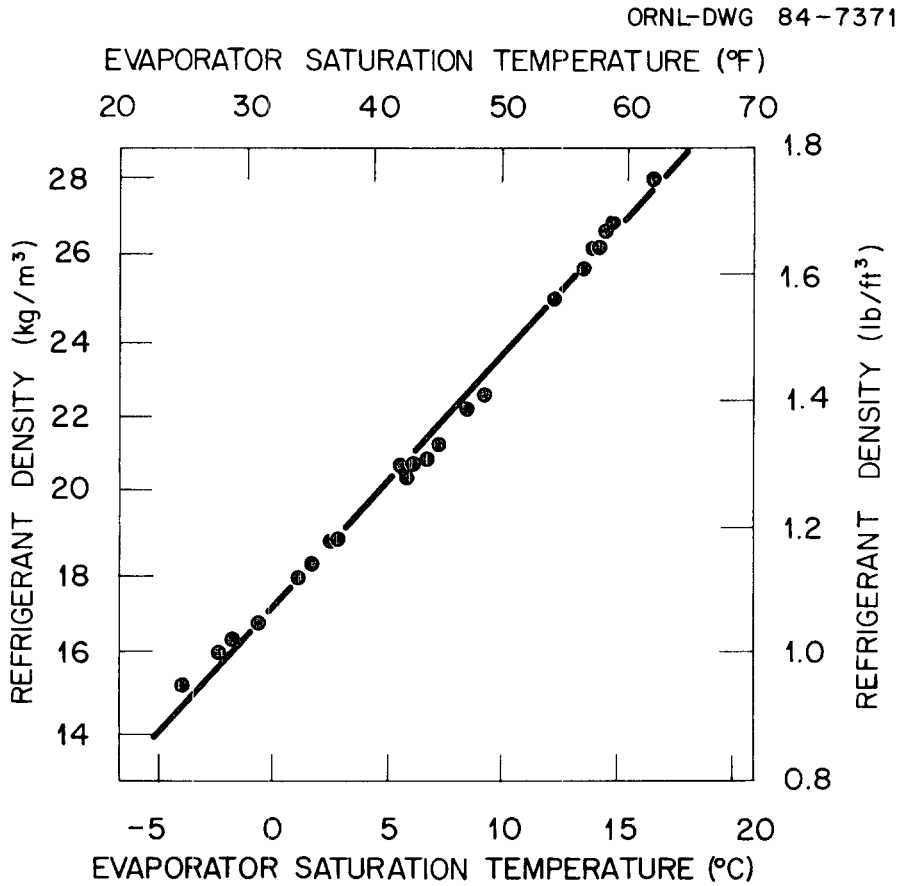

Fig. 12. Effect of evaporator saturation temperature on refrigerant density.

The power input to the fan motor and to the pump are almost independent of ambient temperature change.

Dividing through the right hand side of Eq. 4 by $\dot{m}_r$ results in Eq. 5.

$$\mathrm{COP} = \frac{\Delta h_{\mathrm{cond}}}{\dfrac{\dot{W}_{\mathrm{comp}}}{\dot{m}_r} + \dfrac{(\dot{W}_{\mathrm{fan}} + \dot{W}_{\mathrm{pump}})}{\dot{m}_r}} , \tag{5}$$

where

$\dot{W}_{\mathrm{fan}}$, $\dot{W}_{\mathrm{pump}}$ are previously defined,

Δh_{cond} = enthalpy change through condenser,

$\dot{W}_{\mathrm{comp}}/\dot{m}_r$ = compressor power per unit mass of refrigerant.

The resultant $(\dot{W}_{\mathrm{fan}}, \dot{W}_{\mathrm{pump}})/\dot{m}_r$ term decreases as the ambient temperature rises since $\dot{m}_r$ increases. As previously stated, the required compressor work per unit mass of refrigerant decreases as the ambient temperature increases. Thus the entire denominator of Eq. 3

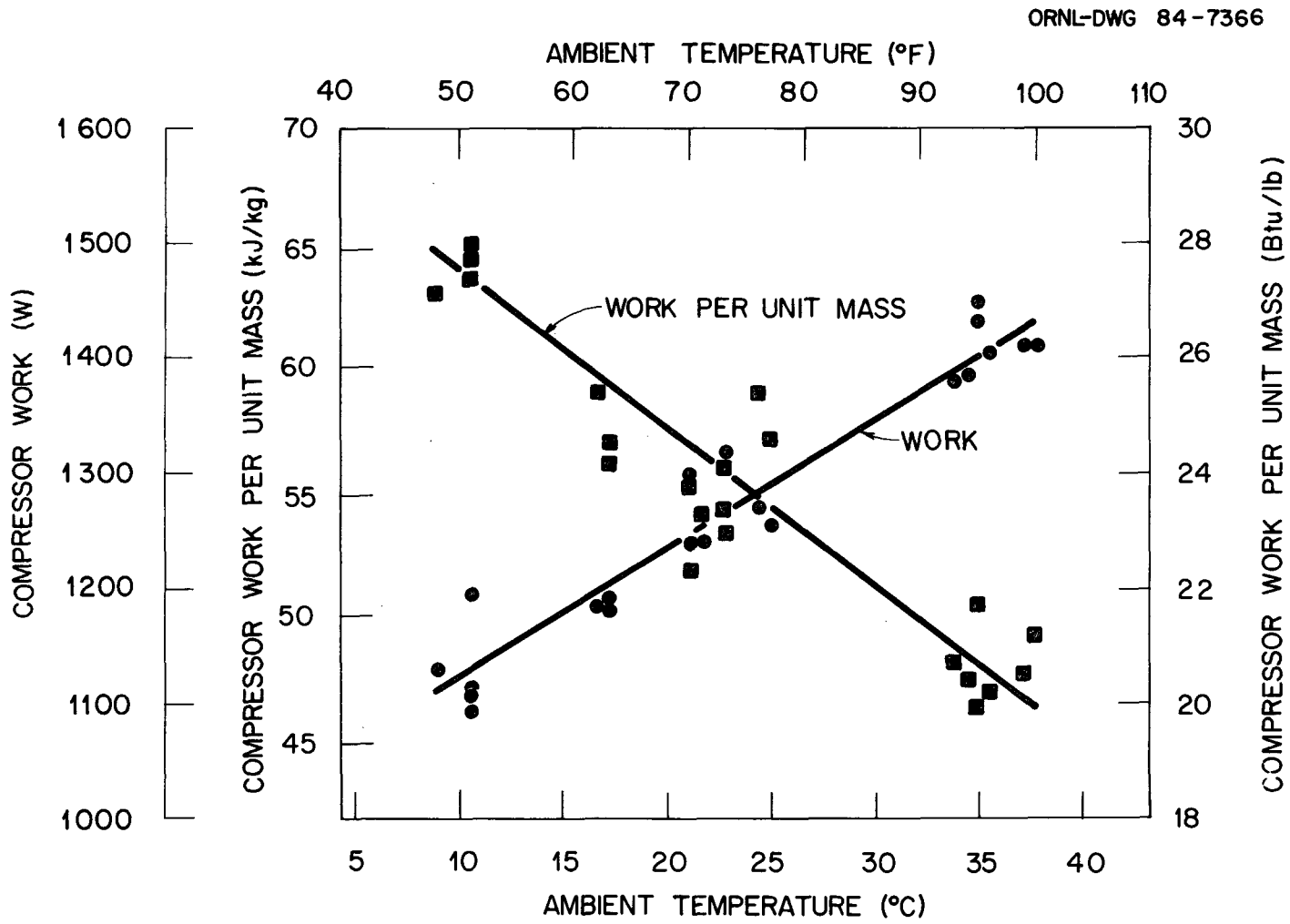

Fig. 13. Effect of ambient temperature on compressor work and compressor work per unit mass of refrigerant required.

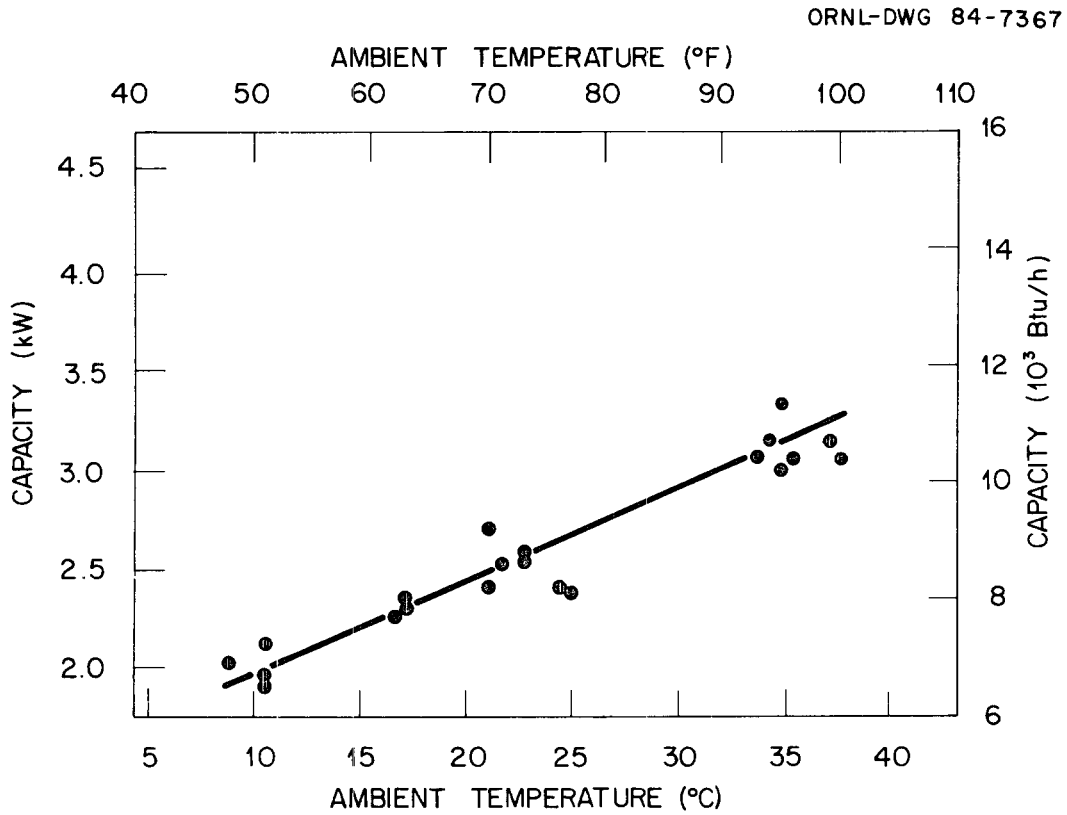

Fig. 14. Effect of ambient temperature on evaporator capacity.

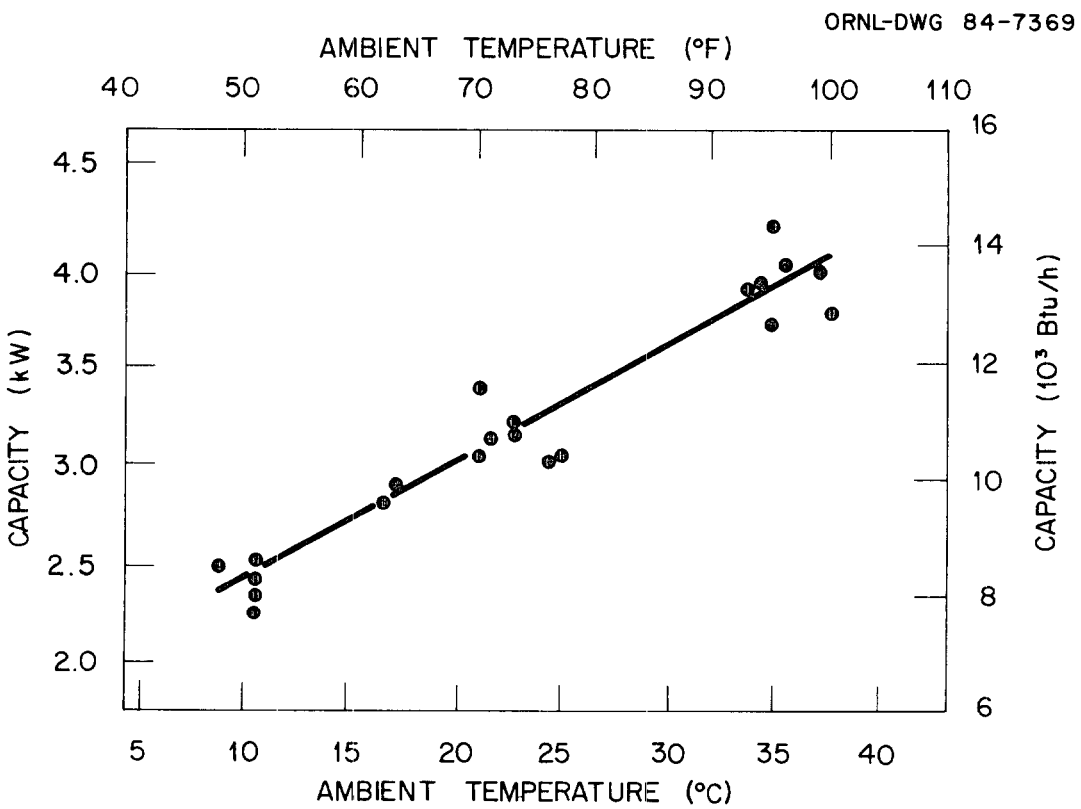

Fig. 15. Effect of ambient temperature on condenser capacity.

decreases at higher ambient temperatures. The enthalpy change through the condenser is shown in Fig. 16 as a function of ambient temperature. As the ambient temperature changes from 10 to 38° C (50 to 100°F), the enthalpy change decreases by just 4%. Thus as the ambient temperature rises, the denominator of the COP equation decreases faster than the numerator decreases resulting in higher values of COP. Figure 17 shows an improvement in the COP of 34% from 1.89 to 2.54 as the ambient temperature changes from 10 to 38°C (50 to 100°F).

The compressor input power is expended in two ways: either transferred to the refrigerant gas in the compressor or lost in heat transfer from the compressor shell. The compressor input power can be expressed as Eq. 6 (ref. 2).

$$\dot{W}_{comp} = \dot{m}_r \delta \Delta_{comp} + \dot{Q}_{can} \ , \tag{6}$$

where

$\dot{m}_r$ is previously defined,

Δh_{comp} = enthalpy change through the compressor,

$\dot{Q}_{can}$ = compressor shell heat loss.

The compressor shell heat loss, calculated from the experimental data, is plotted as a fraction of the compressor input power in Fig. 18 as a function of ambient temperature. As the ambient temperature increases from 10 to 38°C (50 to 100°F), the compressor shell heat

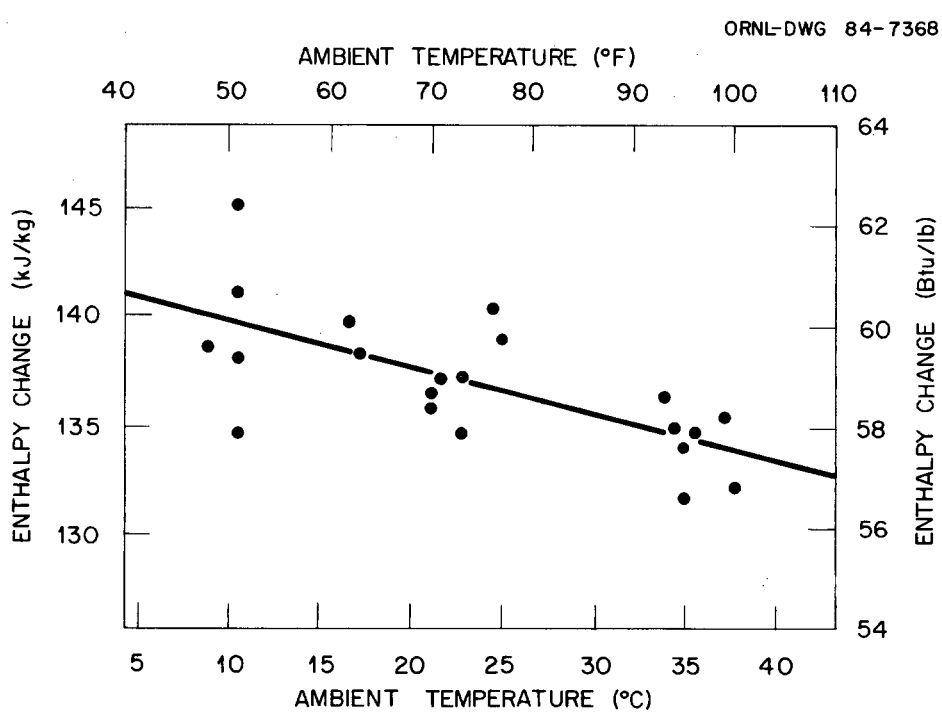

Fig. 16. Effect of ambient temperature on enthalpy change through the condenser.

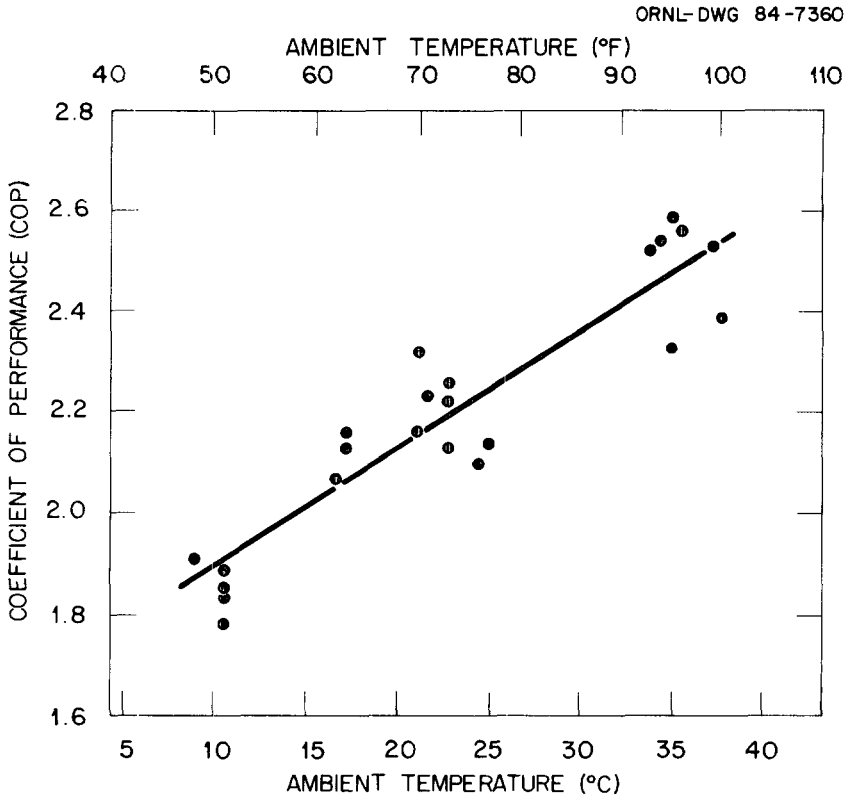

Fig. 17. Effect of ambient temperature on COP.

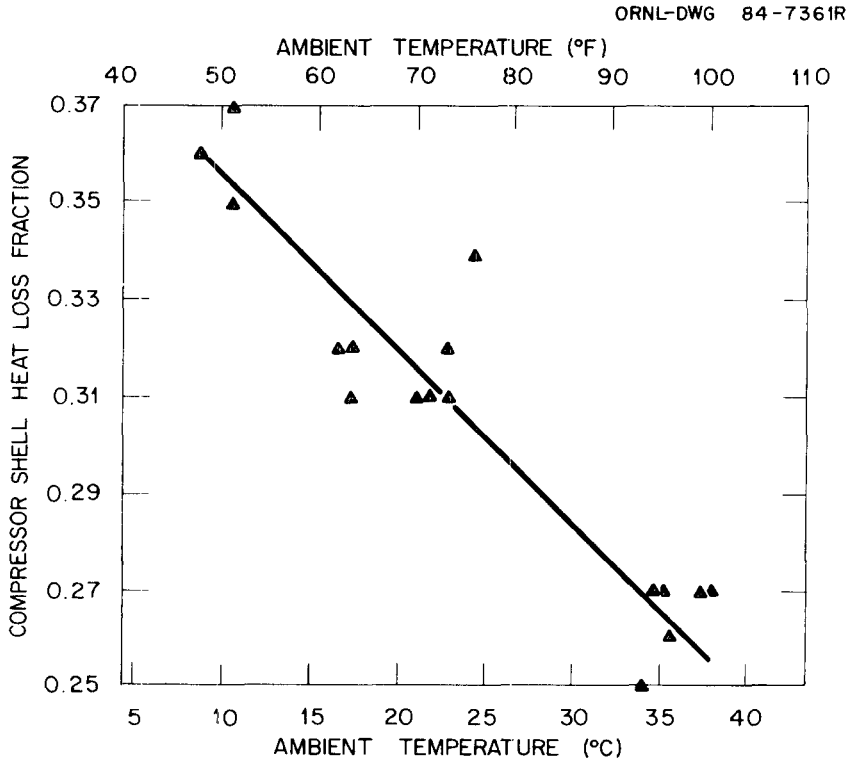

Fig. 18. Effect of ambient temperature on compressor shell heat loss.

loss fraction decreases 28% from 35.5 to 25.5%. The heat loss from the compressor shell heats the air flowing across the evaporator.

The overall calculated isentropic efficiency and volumetric efficiency increase slightly as the ambient temperature increases as indicated in Table 5.

Table 5. Influence of ambient temperature on compressor efficiency

Ambient temperature [°C (°F)]	Power input to compressor [W (Btu/h)]	Isentropic efficiency	Volumetric efficiency
11 (51)	1096 (3740)	0.454	0.759
23 (73)	1316 (4490)	0.477	0.788
34 (93)	1373 (4685)	0.515	0.854

The overall isentropic efficiency given by Eq. 7 (ref. 2) is defined as the ratio of the ideal compressor power to the actual compressor power.

$$\eta = \frac{\dot{m}_r(h_{o,\text{isen}} - h_i)}{\dot{W}_{\text{comp}}} , \tag{7}$$

where

$\dot{m}_r$, $\dot{W}_{\text{comp}}$ are previously defined,

$h_{o,\text{isen}}$ = exit enthalpy for no increase in entropy,

h_i = enthalpy at compressor inlet.

The overall volumetric efficiency given by Eq. 3 is defined as the ratio of the actual volumetric rate of gas moved by the compressor to the ideal pumping rate at rated motor speed.

Rotary compressors have a high volumetric efficiency compared to reciprocating compressors due to the small clearance volume and low re-expansion loss associated with their design.[4] This allows smaller compressor size for a given application.

4.2.3 HPWH Inlet Water Temperature Effect

The graphs described in this section are the results of a steady-state test run at 23°C (73°F) ambient temperature and 75% RH with entering water temperature to the HPWH varying from 115 to 130°F. Some of the raw data is presented in Table A.2 of Appendix A.

Condenser capacity calculations are based on the water-side data and not on the refrigerant-side data due to the refrigerant flowmeter problems that were previously discussed. Evaporator capacity calculations are based on the derived refrigerant-side data and not the air-side data because of insufficient air-side data measurements.

The inlet water temperature is the major driving force in the condenser. As the condenser inlet water temperature increases, the condenser exit saturation temperature increases, causing the enthalpy change through the condenser to decrease slightly as shown in Fig. 19. Enthalpy change across the condenser decreases 4% for the 46 to 54°C (115 to 130°F) water temperature rise. The refrigerant mass flow rate increases slightly, but overall the condenser capacity decreases due to the decreased heat transfer between the water and the refrigerant. As shown in Fig. 20, the condenser capacity decreases 4% as the water temperature increases from 46 to 54°C (115 to 130°F). The total power consumption increases 13% as the entering water temperature rises from 46 to 54°C (115 to 130°F) as shown in Fig. 21. The power input to the pump and fan motor are constant for the water temperature change; therefore, the required compressor work is the only factor causing the total power consumption to increase.

The COP is directly proportional to the decreasing condenser capacity and inversely proportional to the increasing total power consumption. The COP declines 14% from 2.21 to 1.89 for the 46 to 54°C (115 to 130°F) water temperature rise as shown in Fig. 22.

The HPWH inlet water temperature has a small influence on the isentropic compressor efficiency and volumetric compressor efficiency as indicated in Table 6.

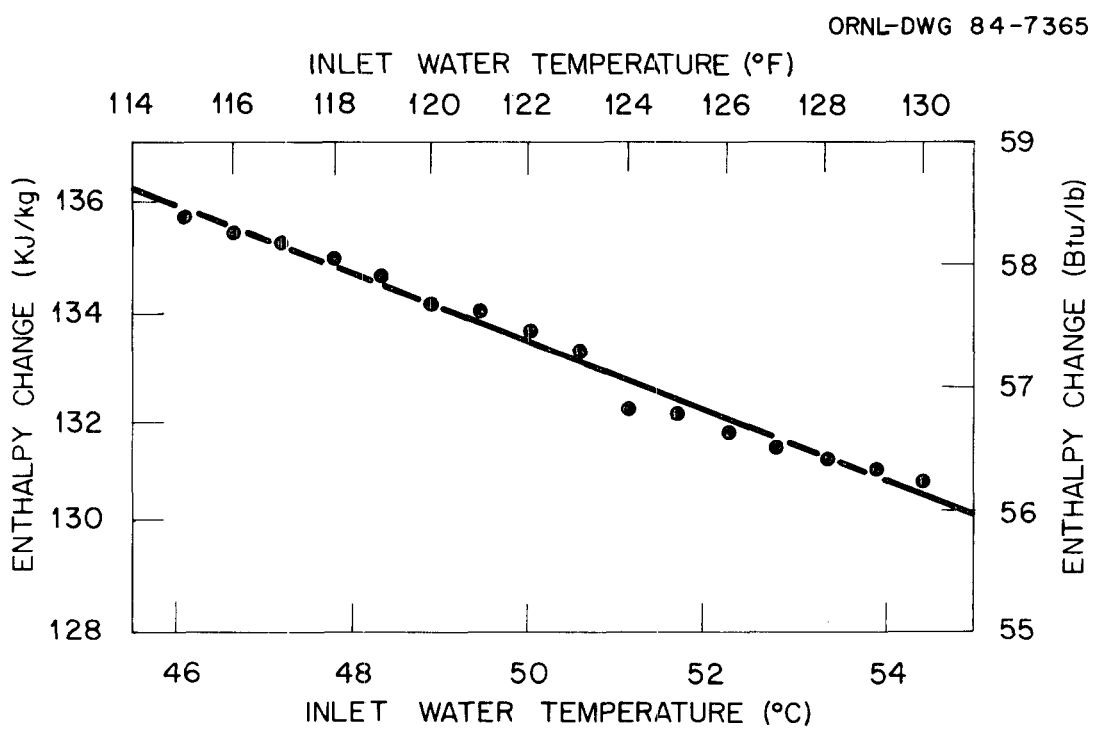

Fig. 19. Effect of HPWH inlet water temperature on enthalpy change through condenser.

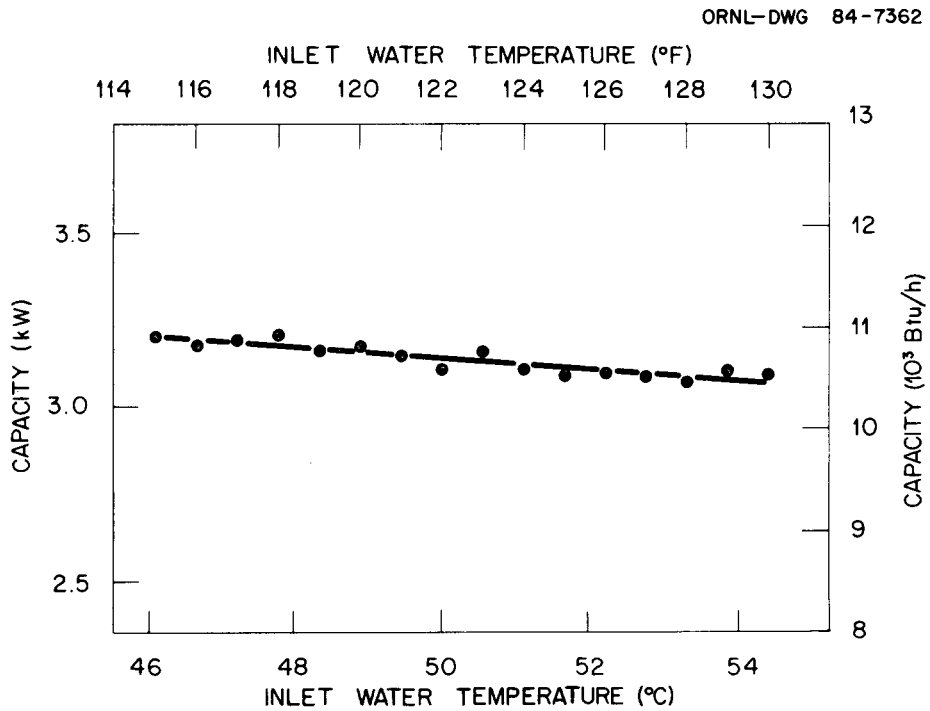

Fig. 20. Effect of HPWH inlet water temperature on condenser capacity.

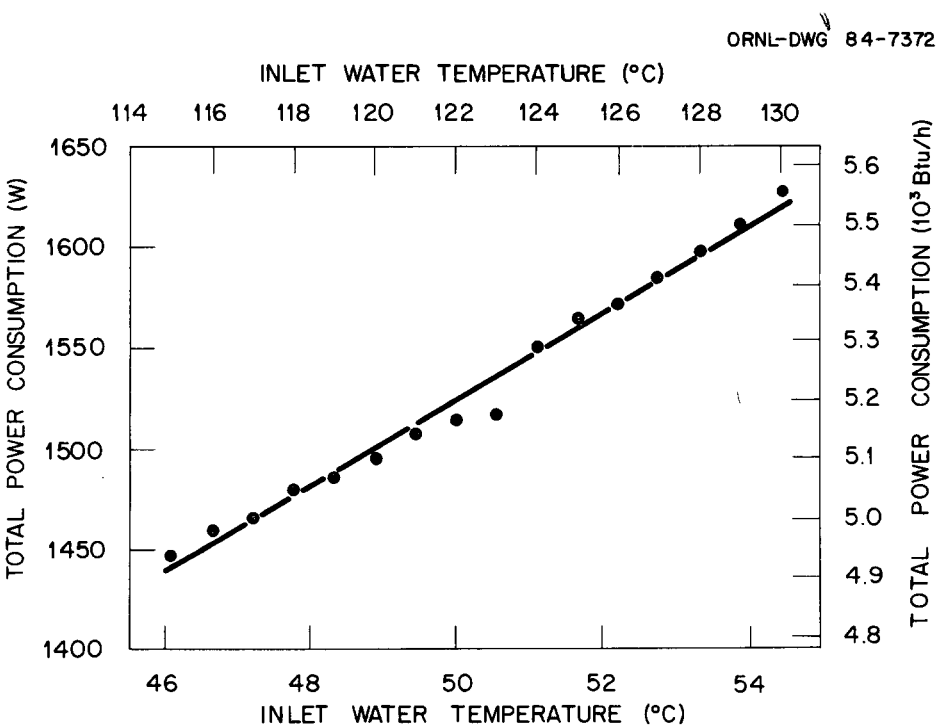

Fig. 21. Effect of HPWH inlet water temperature on total power consumption.

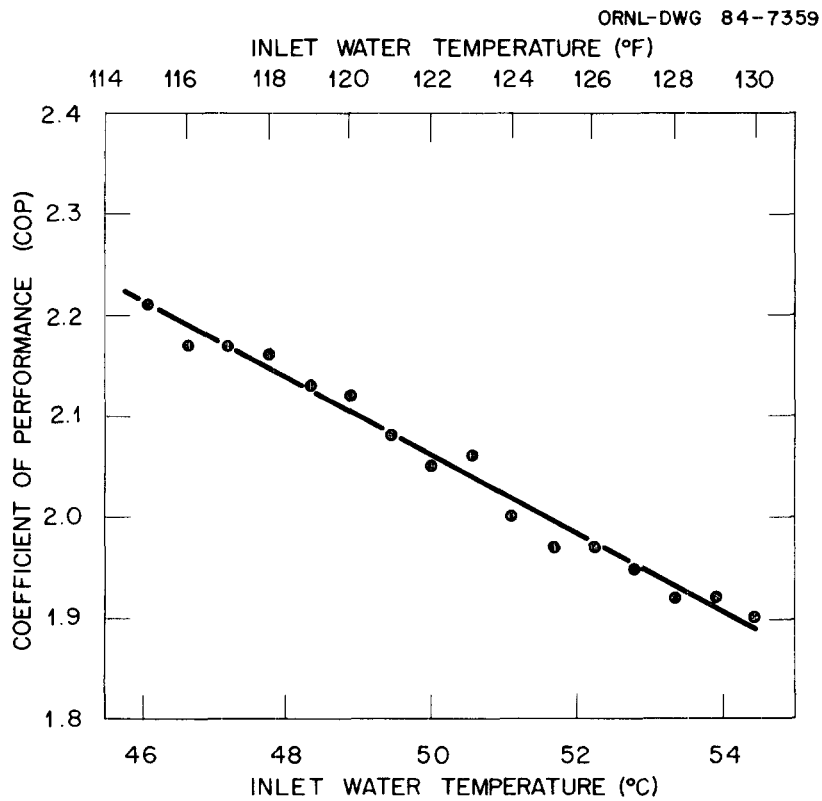

Fig. 22. Effect of HPWH inlet water temperature on COP.

Table 6. Influence of inlet water temperature on compressor efficiency

Inlet water temperature [°C (°F)]	Power input to compressor [W (Btu/h)]	Isentropic efficiency	Volumetric efficiency
47 (116)	1290 (4402)	0.476	0.786
49 (120)	1327 (4528)	0.476	0.787
51 (124)	1380 (4709)	0.471	0.775
53 (128)	1428 (4873)	0.459	0.759

4.2.4 Relative Humidity Effect

The experimental tests were performed in a 60 to 90% and in a 20 to 50% RH condition for each ambient temperature. The high humidity tests listed in Table 7 produced a wet evaporator coil surface. A wet coil compared to a dry coil at the same dry bulb temperature has higher rates of mass transfer because of the added latent heat. Thus the evaporator capacity increases and that results in improved capacity and COP as indicated in Table 7.

Table 7. Influence of relative humidity on performance

Ambient temperature [°C (°F)]	Humidity level	Evaporator capacity [kW (10^3 Btu/h)]	Condenser capacity [kW (10^3 Btu/h)]	COP
11 (51)	Low	1.8 (6.0)	2.3 (7.7)	1.78
11 (51)	High	2.1 (7.1)	2.5 (8.6)	1.84
21 (70)	Low	2.4 (8.2)	3.0 (10.4)	2.16
21 (70)	High	2.7 (9.2)	3.4 (11.6)	2.32
34 (93)	Low	3.1 (10.4)	3.9 (13.3)	2.52
34 (93)	High	3.1 (10.7)	3.9 (13.4)	2.54

5. COMPUTER DESIGN MODEL

The HPWH computer design model is a modification of the ORNL Heat Pump Design Model (ref. 2). This model was selected for use in this project because (1) it is an available comprehensive program that models the major HPWH components, and (2) it has been recently modified to include a water-to-refrigerant condenser model.

The ORNL Heat Pump Design Model is a computer program designed to predict the steady-state performance of conventional vapor-compression, electrically driven, air-to-air heat pumps in heating and cooling modes. It was developed by using physical principles and generalized correlations where possible rather than empirical correlations obtained from manufacturers' literature.

5.1 MODEL MODIFICATIONS

The new subroutines added to the ORNL Heat Pump Design Model are (1) a water-to-refrigerant condenser model developed at Brookhaven National Laboratory (BNL) [2] through work sponsored by DOE and (2) a circulating water pump model developed at ORNL. A description of these routines and their incorporation into the model are explained in the following sections.

A description of the input data format, a sample input data file, and a sample output file for the HPWH computer design model are shown in Appendixes B, C, and D, respectively.

5.1.1 Water-to-Refrigerant Condenser Routine

The water-to-refrigerant condenser model includes both coaxial tube-in-tube and shell-and-tube designs. Data were collected from experimental condenser tests conducted at BNL except for model 100 which was tested at ORNL. All condensers have the required double-wall configuration between the refrigerant and the water. The models were then developed by empirically fitting published heat transfer and pressure drop correlations to these data.

Five different coaxial tube-in-tube condensers, referred to as models 16, 20, 30, 36, and 100, were modeled. The dimensions specific to each condenser needed for input to the HPWH computer design model are given in Table 8. Refer to Fig. 23 and Appendix B for definition of the dimensions given in Table 8. Condenser models 16 and 20 have a roughened outer surface on the inner tube and helical fins on the inside surface. Refrigerant flows in

Table 8. Tube-in-tube condenser dimensions

MODNUM	16	20	30	36	100
TLENTT	186.0	234.0	158.0	173.0	192.0
ENFAC	1.71	1.71	4.24	3.86	1.2
XTEDIA	0.45	0.45	0.645	0.785	0.565
XTBDIA	0.5	0.5	1.044	1.221	0.565
XAEDIA	0.605	0.605	0.715	0.855	0.625
XABDIA	0.645	0.645	1.114	1.291	0.625
XOTDIA	1.055	1.055	1.277	1.388	0.954

ORNL-DWG 85-16598

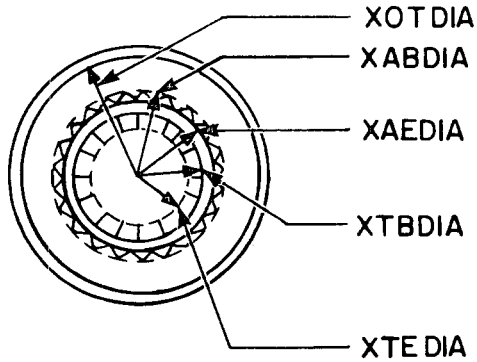

MODELS 16 AND 20

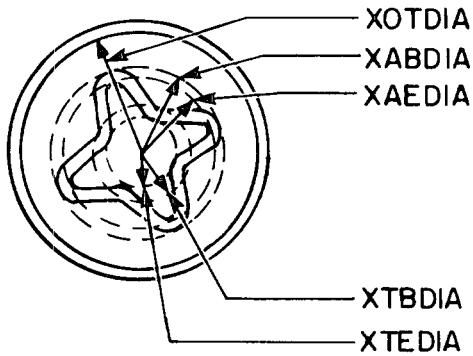

MODELS 30 AND 36

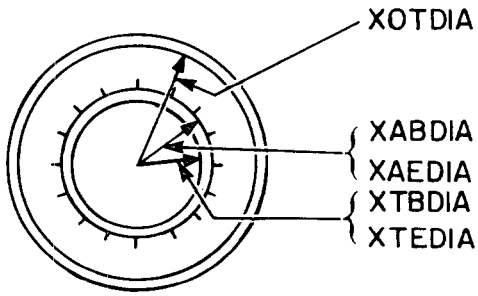

MODEL 100

Fig. 23. Cross section of condenser tubes.

the inner tube countercurrent to the water flowing in the annulus. Condenser models 30 and 36 have helical corrugations in the inner tube. Water flows in the inner tube countercurrent to refrigerant flowing in the annulus. Condenser model 100 has helical fins on the outer surface of the inner tube. Water flows in the inner tube countercurrent to refrigerant flowing in the annulus. Input data for the shell-and-tube condenser are not given because the design is not common in HPWH units. Table 9 gives the coefficients for heat transfer and pressure drop correlations needed in block data of the HPWH computer design model.

Table 9. Tube-in-tube condenser constants

MODNUM	16	20	30	36	100
H1	3.97	4.6	9.0	9.0	1.0
H2	0.741	[a]	0.83	0.83	0.9806
H3	3.7	6.7	5.0	5.0	6.5
H4	1.0	[a]	0.65	0.65	0.0
H5	0.0	[a]	0.12	0.12	0.0
PF1	6.81	9.1	12.0	12.0	33.5

[a]Not applicable.

Because of the type of condenser designs modeled, the HPWH computer design model's use is limited to separated-type HPWH units with similarly designed condensers and is not appropriate for integral-type HPWH units where the condenser is immersed in the water storage tank.

To incorporate the condenser model in the ORNL Heat Pump Design Model, four new routines were added and seven old routines were revised.[6] The new routines and a short description of each follows:

TTCOND — Calculates the refrigerant heat transfer coefficients, total heat transfer, and refrigerant pressure drop for a coaxial tube-in-tube condenser.

STCOND — Calculates the refrigerant heat transfer coefficients, total heat transfer, and refrigerant pressure drop for a shell-and-tube condenser.

GLYPRP — Calculates physical properties of aqueous solutions of ethylene glycol.

FHTPO — Calculates heat transfer coefficients for STCOND.

The revised routines and the changes made in each are as follows:

BLOCK — Assigns values to constants of heat transfer and pressure drop correlations used in the tube-in-tube condenser model. Sets default values for water-to-refrigerant condenser parameters.

CALC — Calculates geometry constants for water-to-refrigerant condenser.

CNDNSR — Calls STCOND and TTCOND.

DATAIN — Reads input data for water-to-refrigerant condenser.

EVAPR — Includes equations to add compressor heat loss to air from evaporator.

OUTPUT — Water-to-refrigerant condenser results are added to printout.

TABLES — Renames variable ITYPE (used in another subroutine) to ITYP.

5.1.2 Circulating Water Pump Routine

A routine modeling the circulating water pump was a necessary addition to the HPWH computer design model. The water flow rate through the condenser and the power input to the pump are needed to calculate the performance of the HPWH unit.

A listing of the routine is shown in Appendix E. The routine begins by calculating the viscosity and density of the water as a function of water temperature. The Reynolds number is calculated and sent to function FRICT to compute the Moody friction factor. The water velocity is calculated from the estimated water flow rate. The water flow rate is a function of the total head present in the system. The power input can also be a function of the total head, but for this specific pump it is a constant.

The total head of a system which a pump must operate against consists of the following components:

1. *Static head*—caused by a difference in elevation of suction and discharge locations.
2. *Friction head*—caused by the flow of fluid through the pipe and fittings.
3. *Velocity head*—caused by a change in velocity of the fluid.
4. *Pressure head*—caused by the suction or discharge locations being under a pressure other than atmospheric.

The reasons for the presence or absence of these different types of heads in the HPWH system are explained below:

1. No static head is present because the HPWH unit connected to the water storage tank is a closed system.
2. The friction head present can be determined by using Darcy's equation, which will be discussed later in this section.
3. No significant velocity head is produced because the water remains at a constant flow rate throughout the system.
4. No pressure head is present because the suction and discharge locations are at atmospheric conditions.

Thus the total head which the pump must operate against is caused by the friction loss in the pipe and fittings. As mentioned previously, Darcy's equation (Eq. 8) is used to calculate this friction loss.

$$H_f = 4f(L/D)(v^2/2g) \ , \tag{8}$$

where

f = the Moody friction factor and is calculated from subroutine FRICT of the model,

v = water velocity and is calculated from the initial estimate of the water flow rate,

g = acceleration of gravity,

L/D = equivalent diameter and is calculated by adding up the friction losses using the equivalent diameter method[7] of the water flow through the pipe, heat exchangers, 90° pipe elbows, and gate valve.

The pressure drop caused by the flowmeter located in the water line was also included in the validation. This pressure drop was determined from the flowmeter manual[8] to be approximately 14 kPa (2.0 psi).

The characteristic curves in Fig. 24 show the relationship of the total head of the pump to the water flow rate and power input to the pump. These curves are obtained from a pump manufacturer and pertain strictly to a specific brand of pump. For this pump, the power input was essentially constant for all water flow rates. The brand of pump installed in the tested HPWH unit is typical of most separated type HPWH units.

In Fig. 25, the pump curve shows the water flow rate for a given pump head. The system curve shows the water flow rate for a given pressure drop in the HPWH water loop. The water pump will always operate at the intersection of these two curves. The function ZERO is used to find the intersection of the curves. Once the water flow rate is determined, the power input to the pump is then calculated.

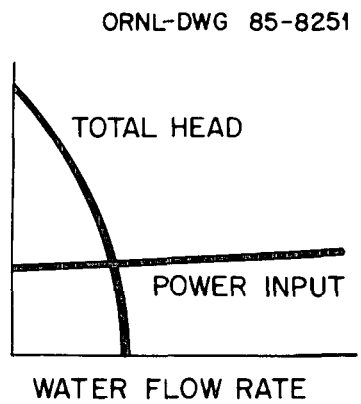

Fig. 24. Circulating Water Pump characteristic curves.

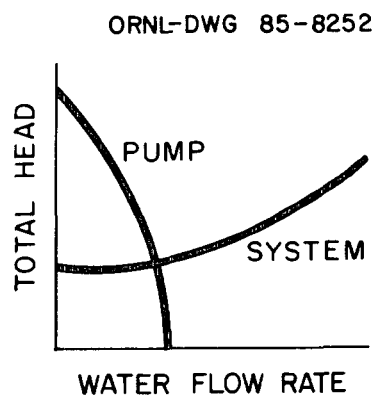

Fig. 25. Pump and system total head curves.

To incorporate the pump routine in the ORNL Heat Pump Design Model, one new routine was added and two old routines were revised. The new routine added was

XMW — Calculates the water flow rate and power input to the circulating water pump.

The revised routines and the changes made in each are as follows:

DRIVER — Calls XMW and assigns values to geometric constants used by XMW.

OUTPUT — Adds XMW results to printout.

5.2 MODEL VALIDATION

Sufficient data were collected from the experimental tests to form a data base on the steady-state performance of the HPWH unit. This data base was used to validate the HPWH computer design model.

The compressor subroutine in the design model is based on biquadratic curve fits to performance curves obtained for a rotary compressor from the compressor manufacturer's calorimeter measurements. These performance curves give compressor power input and refrigerant mass flow rate as functions of refrigerant saturation temperature at compressor shell inlet and exit. The performance curves pertain strictly to the superheat level at which they were generated (20F° superheat). For actual operating conditions (15F° superheat), small correction factors* were applied for adjusting the compressor power input and refrigerant mass flow rate.[9]

Table 10 shows predictions of the compressor map model comparing experimentally measured values of compressor power and refrigerant mass flow rate with the compressor manufacturer's data values and the compressor map curve fit values. Both the compressor

Table 10. Comparison of measured values with compressor map model predictions

Ambient temperature [°C (°F)]	Measured values	Manufacturer's data adjusted	Map curve fit adjusted
Compressor power input, watts			
10.6 (51.0)	1083.5	1019.5	1011.0
21.2 (70.2)	1304.0	1229.8	1234.4
34.3 (93.8)	1406.1	1344.6	1334.9
Refrigerant Mass Flow Rate, kg/h (lb_m/h)[a]			
10.6 (51.0)	61.6 (135.8)	58.6 (129.3)	59.4 (131.0)
21.2 (70.2)	79.1 (174.4)	78.4 (172.9)	78.4 (172.9)
34.3 (93.8)	103.9 (229.0)	106.7 (235.2)	107.0 (236.0)

[a] Derived from measured values.

*These factors were based on reciprocating compressors but were used in this study because of the lack of information on the effect of superheat change in rotary compressors. While some differences between compressor types would be expected, it is assumed here that these would be second-order effects.

manufacturer's data values and compressor map curve fit values have been adjusted for superheat effects. The compressor map curve fit is derived from curve fitting biquadratic equations to the manufacturer's data. The manufacturer's data underestimate the compressor power consumption by an average of 5.3% and slightly underpredict the refrigerant mass flow rate by an average of 1.0% as compared with actual laboratory measurements. This is expected since the manufacturer's data are usually accurate to only ±5%. The compressor power consumption values from the map curve fit are lower than the manufacturer's data values by an average of 0.4%. The refrigerant mass flow rate values from the map curve fit are higher than the manufacturer's data values by an average of 0.6%. Since the map curve fit value of compressor power and refrigerant mass flow rate is used as input into the model, calculated values for these parameters will, thus, be subject to these magnitudes of deviations from the measured values.

The pump head, water flow rate, and power input to the pump were experimentally measured. These measured values and values calculated from the model are shown in Table 11. The calculated pump discharge pressure included a 14 kPa (2.0 psi) pressure drop caused

Table 11. Pump characteristics

	Pump head [m (ft) of water)]	Water flow rate [L/min (gpm)]	Power input to pump [W (Btu/h)]
Measured	2.7 (9.0)	5.22 (1.38)	57.1 (194.8)
Calculated	2.2 (7.2)	9.65 (2.55)	57.0 (194.5)
Corrected	2.8 (9.3)	5.26 (1.39)	57.0 (194.5)

by the water flowmeter as mentioned previously. Since time was not available to determine the reason for the pressure drop differences, an additional amount of pressure drop was added to the pump pressure head to force the water flow rate to equal the measured value. This total amount is listed in Table 11 as the corrected value. Thus for all the validation runs the corrected pump head model was used.

Validation runs were made for the 21.2°C (70.2°F) and for the 34.3°C (93.8°F) ambient cases. Tables 12 and 13 show the comparison between the experimentally measured values and the model calculated values for selected data points and performance results. In both cases the refrigerant, air, and water temperatures agree within 2 to 3C° (4 to 5F°) except for the evaporator inlet temperatures. Also for both cases the refrigerant pressures agree within 10 to 20 kPa (1 to 3 lb/in.^{2}) except for the evaporator inlet pressure. The large disagreements in the evaporator inlet conditions were traced to the model underprediction of the refrigerant pressure drop across the evaporator by approximately 50%. However, since the calculated system balance yields a lower evaporator exit pressure than the measured, it seems likely that the pressure drop underprediction is in the inlet headers to the evaporator and not across the evaporator. Therefore, this underprediction would not significantly affect the evaporator heat transfer calculations.

For the 21.2°C (70.2°F) ambient case, the predicted refrigerant mass flow rate, compressor power input, condenser capacity, and COP are low by 7.8%, 7.5%, 8.4%, and

Table 12. Heat pump water heater model validation at 21.2°C (70.2°F) ambient, 54.1% RH, and 52.6°C (126.6°F) entering water temperature

	Measured	Calculated[a]
Refrigerant temperatures, °C (°F)		
Compressor		
Inlet	14.8 (58.7)	13.1 (55.5)
Exit	93.9 (201.1)	93.3 (199.9)
Condenser		
Inlet	88.8 (191.9)	87.7 (189.9)
Exit	61.0 (141.8)	61.1 (142.0)
TXV inlet	54.4 (129.9)	53.9 (129.1)
Evaporator		
Inlet	12.3 (54.1)	7.7(45.8)
Exit	13.6 (56.4)	11.8 (53.2)
Refrigerant pressures, kPa (psia)		
Compressor		
Inlet	375.1 (54.4)	354.4 (51.4)
Exit	1707.8 (247.7)	1698.2 (246.3)
TXV inlet	1662.3 (241.1)	1687.1 (244.7)
Evaporator inlet	452.3 (65.6)	393.7 (57.1)
ΔP condenser, kPa (psi)	12.4 (1.8)	9.0 (1.3)
ΔP evaporator, kPa (psi)	77.9 (11.3)	37.9 (5.5)
Other temperatures, °C (°F)		
Air, evaporator		
Inlet	20.0 (68.0)	20.0 (68.0)
Exit	12.6 (54.7)	13.6 (56.5)
Water, condenser		
Inlet	52.6 (126.6)	52.6 (126.6)
Exit	60.8 (141.4)	59.9 (139.9)
Compressor power input, W	1304.0	1206.3
Refrigerant mass flow rate, kg/h (lb_m/h)	79.1 (174.4)[b]	72.9 (160.8)
Water flow rate, L/min (gpm)	5.22 (1.38)	5.22 (1.38)
Evaporator capacity, W (Btu/h)	2316.8 (7907.3)	2130.4 (7270.9)
Condenser capacity, W (Btu/h)	2951.9 (10,074.6)	2704.8 (9231.4)
COP[c]	2.000	1.967

[a]Without compressor map corrections.
[b]Derived from measured values.
[c]Includes power input to the fan motor and pump.

1.7%, respectively. For the 34.3°C (93.8°F) ambient case, the predicted refrigerant mass flow rate, compressor power input, condenser capacity, and COP are within +0.9%, −6.7%, −0.9%, and +5.1%, respectively, of the measured values.

The disagreements in the refrigerant mass flow rate and compressor motor power input are mainly due to the compressor map inaccuracies, as previously discussed and shown in Table 10. Therefore experimental data were used to refine the compressor map equations for one case [10.6°C (51.0°F) ambient] to predict the compressor performance more accurately. These corrections allow the accuracy of the heat exchanger predictions to be examined independently of the accuracy of the compressor model predictions.

Table 13. Heat pump water heater model validation at 34.3°C (93.8°F) ambient, 60.7% RH, and 50.1°C (122.1°F) entering water temperature

	Measured	Calculated[a]
Refrigerant temperatures, °C (°F)		
Compressor		
Inlet	22.7 (72.8)	22.1 (71.7)
Exit	93.4 (200.2)	91.6 (196.8)
Condenser		
Inlet	92.1 (197.8)	90.3 (194.6)
Exit	62.9 (145.3)	62.6 (144.6)
TXV inlet	58.7 (137.7)	58.4 (137.1)
Evaporator		
Inlet	20.3 (68.5)	17.4 (63.4)
Exit	21.4 (70.6)	20.9 (69.6)
Refrigerant pressures, kPa (psia)		
Compressor		
Inlet	475.7 (69.0)	466.8 (67.7)
Exit	1754.0 (254.4)	1726.4 (250.4)
TXV inlet	1685.1 (244.4)	1703.7 (247.1)
Evaporator inlet	570.9 (82.8)	527.4 (76.5)
ΔP condenser, kPa (psi)	15.9 (2.3)	18.6 (2.7)
ΔP evaporator, kPa (psi)	95.8 (13.9)	57.9 (8.4)
Other temperatures, °C (°F)		
Air, evaporator		
Inlet	31.8 (89.2)	31.7 (89.1)
Exit	21.5 (70.7)	24.4 (76.0)
Water, condenser		
Inlet	50.1 (122.1)	50.1 (122.1)
Exit	61.1 (142.0)	60.6 (141.1)
Compressor power input, W	1406.1	1311.8
Refrigerant mass flow Rate, kg/h (lb_m/h)	103.9 (229.0)[b]	104.8 (231.1)
Water flow rate, L/min (gpm)	5.11 (1.35)	5.19 (1.37)
Evaporator Capacity, W (Btu/h)	3004.6 (10,254.6)	3037.4 (10,366.7)
Condenser Capacity, W (Btu/h)	3874.5 (13,223.4)	3838.3 (13,100.0)
COP[c]	2.470	2.596

[a]Without compressor map corrections.
[b]Derived from measured values.
[c]Includes power input to fan motor and pump.

Table 14 shows the measured values and the model-calculated values with and without compressor map corrections for various data points and performance results of the 10.6°C (51.0°F) ambient temperature case. As with the previous validation cases, the temperatures and pressures are in good agreement except for the evaporator conditions due to the underprediction by the model of the refrigerant pressure drop across the evaporator. Table 15 shows the percentage difference between the measured values and the model-calculated values with and without the compressor map corrections for the refrigerant mass flow rate, compressor power input, condenser capacity, and COP. The compressor map corrections do improve the predictions of refrigerant mass flow rate, compressor power input, and condenser capacity, with the COP differences becoming a little larger due to offsetting differences in power and capacity.

Table 14. Heat pump water heater model validation at 10.6°C (51.0°F) ambient, 66% RH, and 46.9°C (116.4°F) entering water temperature

	Measured	Calculated[a]	Calculated[b]
Refrigerant temperatures, °C (°F)			
Compressor			
Inlet	6.3 (43.3)	5.5 (41.9)	5.2 (41.4)
Exit	86.1 (187.0)	85.6 (186.1)	87.4 (189.4)
Condenser			
Inlet	79.4 (175.0)	78.4 (173.2)	80.4 (176.8)
Exit	52.9 (127.2)	53.4 (128.2)	53.8 (128.8)
TXV inlet	43.6 (110.4)	43.4 (110.2)	44.1 (111.3)
Evaporator			
Inlet	3.8 (38.9)	0.1 (32.1)	0.0 (32.0)
Exit	4.8 (40.6)	4.0 (39.2)	3.7 (38.6)
Refrigerant pressures, kPa (psia)			
Compressor			
Inlet	286.1 (41.5)	278.5 (40.4)	275.8 (40.0)
Exit	1446.5 (209.8)	1453.4 (210.8)	1463.1 (212.2)
TXV inlet	1414.8 (205.2)	1447.9 (210.0)	1447.9 (210.0)
Evaporator inlet	348.9 (50.6)	309.6 (44.9)	308.9 (44.8)
ΔP condenser, kPa (psi)	12.4 (1.8)	3.4 (0.5)	4.1 (0.6)
ΔP evaporator, kPa (psi)	60.0 (8.7)	29.6 (4.3)	31.7 (4.6)
Other temperatures, °C (°F)			
Air, evaporator			
Inlet	9.9 (49.9)	9.9 (49.9)	9.9 (49.8)
Exit	4.4 (39.9)	5.2 (41.4)	5.1 (41.2)
Water, condenser			
Inlet	46.9 (116.4)	46.9 (116.4)	46.9 (116.4)
Exit	53.5 (128.3)	52.9 (127.3)	53.2 (127.7)
Compressor power input, W	1083.5	1001.5	1069.1
Refrigerant mass flow rate, kg/h (lb_m/h)	61.6 (135.8)[c]	57.5 (126.7)	59.2 (130.5)
Water flow rate, L/min (gpm)	5.22 (1.38)	5.19 (1.37)	5.19 (1.37)
Evaporator Capacity, W (Btu/h)	1931.0 (6590.4)	1797.3 (6134.2)	1838.5 (6274.8)
Condenser Capacity, W (Btu/h)	2376.5 (8110.8)	2194.8 (7490.9)	2279.9 (7781.1)
COP[d]	1.900	1.879	1.845

[a]Without compressor map corrections.
[b]With compressor map corrections.
[c]Derived from measured values.
[d]Includes power input to fan motor and pump.

Table 15. Percent difference between the model calculated values (without and with the compressor map corrections) and the measured values at 10.6°C (51.0°F) ambient

	Refrigerant mass flow rate	Compressor power input	Condenser capacity	Coefficient of performance
Without correction	−6.7	−7.6	−7.6	−1.1
With correction	−3.9	−1.3	−4.1	−2.9

6. RECOMMENDATIONS

Now that the model has been validated and proved capable of predicting the performance of the HPWH system reasonably well, the next step should be to use the design model in a parametric study.[10] Following is a list of potential design parameters for such a study that would provide an analytical capability to evaluate the effect of improved components or new design features on the HPWH system performance:

- condenser length,
- condenser tube diameter,
- refrigerant subcooling at condenser exit,
- evaporator tube diameter,
- number of evaporator tube rows,
- number of evaporator refrigerant circuits,
- compressor displacement,
- water flow rate, and
- air flow rate.

Caution should be exercised in selecting the most meaningful combinations of these variables. Plots should be generated showing COP as a function of two design parameters varied about their base case value.

The water circulating pump model is based on the characteristic curve of one specific pump. It is not a generalized equation as previously discussed. The pump model would be more useful in parametric studies if it were generalized similar to the outdoor fan model[2] by using specific speed versus efficiency curves. This method would allow various pump sizes, speeds, and water flow rates to be considered and provide proper pump efficiencies. The model could then be used to find the best pump (one that requires the least amount of energy) to match the system conditions selected.

Another design approach that should be undertaken is optimization. An optimizing program has been used with success with the ORNL Heat Pump Design Model.[11,12] The program allows the simultaneous optimization of selected design variables while constraining other parameters to constant values or within specific limits. For the HPWH study, the parameters previously mentioned for the parametric study should be optimized simultaneously while holding the condenser capacity constant. In this way, maximum performance would be sought at a fixed unit size.

The HPWH computer design model is available upon request to those involved in HPWH design.

7. REFERENCES

1. *Fed. Regist.*, **49**(27), (Feb. 8, 1984).

2. S. K. Fischer and C. K. Rice, *The Oak Ridge Heat Pump Models: 1. A Steady-State Computer Design Model for Air-to-Air Heat Pumps*, ORNL/CON-80/R1, Oak Ridge National Laboratory, Oak Ridge, Tenn., August 1983.

3. R. L. Dunning, F. R. Amthor, and E. J. Doyle, *Research and Development of a Heat Pump Water Heater*, ORNL/Sub-7321/2, Energy Utilization Systems, Inc., Pittsburgh, Penn. August 1978.

4. American Society of Heating, Refrigeration, and Air-Conditioning, 1983 Equipment Volume, Chapter 12, p. 12.12.

5. M. Catan et al, *Optimized Ground Coupled Heat Pump Design, Phase I Final Report*, BNL-51957, Brookhaven National Laboratory, Upton, N.Y., October 1985.

6. V. D. Baxter, Oak Ridge National Laboratory, Oak Ridge, TN, personal communication to K. H. Zimmerman, Oak Ridge National Laboratory, Oak Ridge, Tenn., January 1985.

7. Baumeister, Avallone and Baumeister, eds., *Marks' Standard Handbook for Mechanical Engineers*, Eighth Edition, 1958, p. 3-58.

8. Flow Technology, Inc., *Installation and Maintenance Manual*, Industrial Omniflo Turbine Flowmeter Model FTO, Phoenix, Ariz. May 1981, p. 5.

9. A. E. Dabiri and C. K. Rice, "A Compressor Simulation Model with Corrections for the Level of Suction Gas Superheat," *ASHRAE Trans.*, **87**, Part II, 1981.

10. K. H. Zimmerman, "Laboratory Test, Design Model Validation, and Parametric Study of a Heat Pump Water Heater," Proceedings of the 7th Heat Pump Technology Conference, Oklahoma State University, Tulsa, October 15-16, 1984.

11. C. K. Rice et al., "Design Optimization of Conventional Heat Pumps: Application to Steady-State Heating Efficiency," *ASHRAE Trans.*, **87** (Pt. 1) (1981).

12. S. K. Fischer and C. K. Rice, "System Design Optimization and Validation for Single-Speed Heat Pumps," *ASHRAE Trans.*, **91**, 1985.

Appendix A

EXPERIMENTAL DATA

Table A.1. Performance data for steady-state tests run under various ambient conditions

Date	Ambient conditions		Water temperature (°F) Condenser		Flow rates	
	Temperature (°F)	RH (%)	In	Out	Refrigerant (lb/h)	Water (gpm)
10/31/83	51.0	65.7	120.4	132.2	135.3	1.38
2/22/84	51.0	97.6	119.7	132.5	149.1	1.37
10/28/83	70.6	52.4	119.8	135.2	177.1	1.37
10/25/85	70.2	87.4	119.8	136.7	198.4	1.39
9/28/83	92.9	29.9	120.1	139.6	226.4	1.38
9/23/83	93.8	60.6	120.2	140.3	231.7	1.36

Refrigerant temperature (°F)

Compressor		Condenser		TXV		Evaporator	
In	Out	In	Out	In	Out	In	Out
44.4	191.4	179.4	130.8	114.2	40.7	39.9	41.6
47.4	193.0	172.7	128.4	112.1	44.9	44.2	44.7
58.0	194.9	185.8	136.3	124.9	54.4	53.5	55.6
64.9	195.2	188.8	138.5	128.3	60.2	59.5	63.2
68.6	199.8	195.3	140.9	130.8	66.0	65.0	66.1
72.6	198.8	196.2	143.8	136.5	69.2	68.2	70.0

Table A.1 (continued)

Refrigerant pressures					
Absolute (psia)				Differential (psi)	
Compressor		TXV	Evaporator	Condenser	Evaporator
In	Out	in	in	DP	DP
42.2	219.1	214.4	51.5	1.8	8.9
46.1	225.3	220.4	55.7	1.8	9.3
53.9	231.6	224.9	65.0	1.9	11.2
59.7	238.3	230.5	71.8	2.1	12.1
65.5	249.6	240.5	78.4	2.3	13.0
68.6	249.6	239.6	82.3	2.4	13.7

Power inputs (W)			Performance	
Compressor	Fan motor	Pump	Condenser capacity (Btu/h)	COP
1117.8	110.5	55.9	8008.8	1.83
1171.6	115.8	59.1	8694.0	1.89
1241.2	111.1	57.1	10386.6	2.16
1297.6	111.9	57.0	11584.8	2.32
1373.3	111.0	57.1	13272.0	2.52
1387.1	109.8	56.1	13440.6	2.54

Table A.2. Performance data for a steady-state test run at various entering water temperatures

Date	Ambient conditions		Water temperature (°F) Condenser		Flow rates	
	Temperature (°F)	RH (%)	In	Out	Refrigerant (1b/h)	Water (gpm)
2/28/84	73.3	71.7	118.2	134.3	186.6	1.37
	73.2	73.9	120.2	136.3	187.0	1.37
	73.2	74.4	122.2	138.2	186.4	1.37
	73.2	75.3	124.2	140.0	186.0	1.38
	73.3	74.4	126.1	141.9	186.4	1.38
	73.2	76.0	128.3	143.9	186.6	1.38
	73.5	76.4	130.2	145.8	186.6	1.38
	73.5	78.8	132.1	147.7	186.0	1.37
	73.7	78.1	134.1	149.6	187.5	1.38

Refrigerant temperatures (°F)

Compressor		Condenser		TXV		Evaporator	
In	Out	In	Out	In	Out	In	Out
62.8	196.4	183.0	134.6	122.8	58.0	57.2	60.5
63.0	199.0	185.3	136.5	124.4	58.3	57.5	65.8
63.2	201.2	187.3	138.2	125.9	58.5	57.7	61.0
63.8	202.9	189.1	139.9	127.4	58.9	58.1	61.6
63.6	204.3	189.5	141.1	128.4	58.6	57.8	61.6
64.6	207.1	192.0	143.6	130.5	59.6	58.8	62.5
65.1	209.6	194.6	145.5	132.2	60.3	59.4	63.0
65.8	212.3	197.1	147.4	134.0	60.8	60.0	63.6
66.2	215.3	199.8	149.3	135.8	61.3	60.4	64.1

Table A.2 (continued)

Refrigerant pressures					
Absolute (psia)				Differential (psi)	
Compressor		TXV	Evaporator		
In	Out	in	in	Condenser DP	Evaporator DP
58.0	235.4	228.5	69.2	2.2	11.3
58.3	240.3	233.4	69.5	2.2	11.4
58.4	245.2	238.2	69.7	2.1	11.5
58.9	250.0	243.1	70.3	2.1	11.5
58.4	252.9	245.9	70.0	2.1	11.7
59.6	260.5	253.6	71.1	2.1	11.6
60.0	265.9	258.9	71.7	2.0	11.8
60.7	271.4	264.4	72.4	2.0	11.7
61.2	276.7	269.7	73.0	2.0	11.9

Power inputs (W)			Performance	
Compressor	Fan motor	Pump	Condenser capacity (Btu/h)	COP
1277.8	112.8	57.5	10896.0	2.21
1297.2	111.8	57.2	10878.0	2.17
1316.2	112.5	57.5	10792.8	2.13
1338.1	113.1	57.5	10717.2	2.08
1346.6	112.4	57.5	10680.6	2.06
1380.0	112.4	57.3	10599.6	2.00
1401.0	112.3	57.6	10567.8	1.97
1428.2	112.7	57.0	10493.4	1.92
1458.5	112.4	57.2	10545.6	1.90

Appendix B

DESCRIPTION OF INPUT DATA FORMAT

TITLE, OUTPUT, and MODE DATA:

CARD #1		FORMAT (20A4)	
	ITITLE	Descriptive title for system described by this set of data	SAMPLE
CARD #2		FORMAT (8I10)	
	LPRINT	Output switch to control the detail of printed results: =0, for minimum output with only an energy input and output summary printed =1, for a summary of the system operating conditions and component performance calculations as well as the energy summary =2, for output after each intermediate iteration converges =3, for continuous output during intermediate iterations	1
CARD #3		FORMAT (8I10)	
	NCORH	Switch to specify cooling or heating mode =1, for cooling mode =2, for heating mode*	1
	**ITYPE	Switch to specify type of condenser =0, air-to-refrigerant =1, liquid-to-refrigerant	1
	**MODNUM	Switch to specify type of liquid-to-refrigerant heat exchanger =0, shell-and-tube >0, tube-in-tube (16, 20, 30, 36, 100)	100

SUPERHEAT / CHARGE INVENTORY DATA:

CARD #4		FORMAT (I10,7F10.4)	
	ICHRGE	Switch for specifying compressor inlet superheat or system refrigerant charge =0, specify refrigerant superheat (or quality) and compute the required system refrigerant charge =1, estimate compressor inlet superheat and specify the system refrigerant charge	0
	SUPER	if ICHRGE=0, the specified refrigerant superheat or quality) at the compressor shell inlet (F deg. or negative of the desired quality fraction);	15.79

*In its present form, the HPWH design model cannot be run in heating mode because there are no evaporating correlations given in the liquid-to-refrigerant heat exchanger model.

**Additions and/or changes for HPWH design model.

if ICHRGE=1, an estimate of refrigerant superheat or quality) at the compressor shell inlet (F deg. or negative of the desired quality fraction)

Variables Used Only if ICHRGE=1

REFCHG	Specified system refrigerant charge (lb_m)
ACCVOL	internal void space volume of the accumulator ($in.^3$)
ACLVOL	maximum liquid volume in the accumulator ($in.^3$)
CMPVOL	void space volume in the compressor can ($in.^3$)

FLOW CONTROL DEVICE DATA:
the variables on this card depend on the type of flow control device selected.

CARD #5 FORMAT (I10,7F10.4)

Fixed Condenser Subcooling:

IREFC	=0, for specified refrigerant subcooling at the condenser exit	0
DTROC	the specified refrigerant subcooling (or quality) at the condenser exit (F deg. or negative of the desired quality fraction)	7.0

Thermostatic Expansion Valve:

IREFC	=1, for the thermostatic expansion valve	1
TXVRAT	The rated capacity of the TXV (tons)	2.0
STATIC	The static superheat setting for the TXV (°F)	6.0
SUPRAT	The TXV superheat at rating conditions (°F)	11.0
BLEEDF	The TXV bypass or bleed factor	1.15
NZTBOP	A switch to omit TXV nozzle and tube pressure drop calculations, =0.0, to omit tube and nozzle pressure drops =1.0, to include tube and nozzle pressure drop calculations	0.0

Capillary Tube:

IREFC	=2, for a capillary tube expansion device	2
CAPFLO	the capillary tube flow factor, see ASHRAE Guide and Data Book, Equipment Vol. (1975), Fig. 41, pp. 20-25.	2.2
NCAP	the number of capillary tubes in parallel	1.0

Short-Tube Orifice:

IREFC	=3, for a short-tube orifice	3
ORIFD	the diameter of the short-tube orifice (inches)	0.0544

ESTIMATES of the LOW and HIGH SIDE REFRIGERANT SATURATION TEMPERATURES:

CARD #6 FORMAT (8F10.4)

TSICMP	estimate of the refrigerant saturation temperature at the compressor inlet (°F)	42.9
TSOCMP	estimate of the refrigerant saturation temperature at the compressor outlet (°F)	149.45

COMPRESSOR DATA:

CARD #7		FORMAT (I10,7F10.4)	
	ICOMP	switch to specify which compressor submodel is to be used, =1, for the efficiency and loss model, =2, for the map-based submodel.	2
	DISPL	total compressor piston displacement (in.^{3})	1.428
	SYNC	the synchronous compressor motor speed when ICOMP=1 and FLMOT is specified on card #9, the rated compressor motor speed (rpm) when ICOMP=1 and FLMOT is to be calculated or when ICOMP=2	(3600.) 3450.
	QCAN	compressor shell heat loss rate (Btu/h), used if CANFAC is 0.0	0.0
	CANFAC	Switch to control the method of specifying the compressor shell heat loss rate, QCAN =0.0, to specify QCAN explicitly <1.0, to calculate QCAN as a fraction of the compressor input power, POW, (i.e., QCAN = CANFAC * POW) =>1.0, to calculate QCAN from empirical fit: QCAN = 0.90 * (1-motor*mechanical efficiency) * POW	0.33

EFFICIENCY AND LOSS MODEL COMPRESSOR DATA:

CARD #8		FORMAT (8F10.4)	
	VR	Compressor actual clearance volume ratio	0.06
	EFFMMX	Maximum efficiency of the compressor motor	0.82
	ETAISN	Isentropic efficiency of the compressor	0.70
	ETAMEC	Mechanical efficiency of the compressor	0.80

CARD #9		FORMAT (I10,7F10.4)	
	MTRCLC	Switch to determine whether to calculate the full load motor power (FLMOT) or to use the input value =0, to calculate FLMOT =1, to use the input value of FLMOT	0
	FLMOT	Compressor motor output at full load (kW) (not used if MTRCLC=1)	(2.15)
	QHILO	Heat transfer rate from the compressor inlet line to the inlet gas (Btu/hr), used if HILOFC=0.0	300.0
	HILOFC	Switch to determine internal heat transfer from the high side to the low side, QHILO =0.0, to specify QHILO explicity <1.0, to calculate QHILO = HILOFC * POW =>1.0, to calculate QHILO = 0.03 * POW	0.0

OR MAP-BASED COMPRESSOR MODEL INPUT DATA:

CARD #8		FORMAT (8E10.3)	
	CPOW (1)	Coefficient for the second order term in condensing temperature for the compressor power consumption	4.533E−05
	CPOW (2)	Coefficient for the linear term in condensing temperature for the compressor power consumption	−9.219E−03
	CPOW (3)	Coefficient for the second order term in evaporating temperature for the compressor power consumption	−9.168E−05
	CPOW (4)	Coefficient for the linear term in evaporating temperature for the compressor power consumption	−6.056E−03
	CPOW (5)	Coefficient for the cross-term in condensing and evaporating temperatures for the compressor power consumption	1.375E−04
	CPOW (6)	Constant term in the fit to compressor power consumption as a function of condensing and evaporating temperatures (KW)	1.151E+00
	DISPLB	Base compressor displacement for the compressor map (in.^{3})	1.430E+00
	SUPERB	Base "superheat" value for the compressor map if positive, the base superheat entering the compressor (F deg.)	20.00E+00
		if negative, the negative of the return gas temperature into the compressor (°F)	(−95.00E+00)

CARD #9		FORMAT (8E10.3)	
	CXMR (1)	Coefficient for the second order term in condensing temperature for the fit to refrigerant mass flow rate	−2.742E−03
	CXMR (2)	Coefficient for the linear term in condensing temperature for the fit to refrigerant flow rate	3.918E−01
	CXMR (3)	Coefficient for the second order term in evaporating temperature for the fit to refrigerant mass flow rate	4.301E−02
	CXMR (4)	Coefficient for the linear term in evaporating temperature for the fit to refrigerant mass flow rate	1.312E+00
	CXMR (5)	Coefficient for the cross-term in condensing and evaporating temperatures for the fit to refrigerant mass flow rate	−6.953E−03
	CXMR (6)	Constant term in the fit to refrigerant mass flow rate as a quadratic function in both the condensing and evaporating temperatures (lb_m)	8.350E+01

EVAPORATOR DATA:

CARD #10		FORMAT (8F10.4)	
	TAII	Air temperature entering the heat exchanger (°F)	68.0
	RHI	Relative humidity of the air entering the heat exchanger	0.541

CARD #11		FORMAT (8F10.4)	
	QA	Air flow rate (cfm)	525.
	FANEF	<=1.0, the specified value of the combined fan-fan motor efficiency	(0.153)
		>1.0, the specified value of the fan power (watts)	111.9
	DDUCT	Diameter of each of six indentical air ducts with equivalent lengths of 100 ft. (in.)	1000.0
	FIXCAP	House heating load (Btu/h), used to calculate the necessary backup resistance heat in heating mode	0.0
CARD #12		FORMAT (8F10.4)	
	AAF	Frontal area of the coil (ft^2)	1.7778
	NT	Number of refrigerant tube rows in the direction of the air flow	2.0
	NSECT	Number of equivalent, parallel refrigerant circuits in the heat exchanger	2.0
	WT	Spacing of the refrigerant tubes in the direction of the air flow (in.)	0.625
	ST	Spacing of the refrigerant tube passes perpendicular to the direction of air flow (in.)	1.00
	RTB	Total number of return bends in the heat exchanger (all circuits)	29.0
CARD #13		FORMAT (8F10.4)	
	FINTY	Switch to specify the type of fin surface, =1.0, for smooth fins =2.0, for wavy fins =3.0, for louvered fins	2.0
	FP	Fin pitch (fins/in.)	14.0
	DELTA	fin thickness (in.)	0.0045
	DEA	Outside diameter of the refrigerant tubes (in.)	0.3120
	DER	Inside diameter of the refrigerant tubes (in.)	0.2890
	XKF	Thermal conductivity of the fins (Btu/h-ft-F)	128.3
	XKT	Thermal conductivity of the tubes (Btu/h-ft-F)	196.0
	HCONT	Fraction of the default computed contact conductance between the fins and tubes	1.0

CONDENSER DATA:

**CARD #14		FORMAT (8F10.4)	
	TLENTT	total length of heat exchanger tubes (in.)	192.0
	ENFAC	heat transfer enhancement factor	1.20
**CARD #15		FORMAT (8F10.4)	
	XTEDIA	inside diameter of inner tube, min (in.)	0.565
	XTBDIA	inside diameter of inner tube, max (in.)	0.565
	XAEDIA	outside diameter of inner tube, min (in.)	0.625
	XABDIA	outside diameter of inner tube, max (in.)	0.625
	XOTDIA	inside diameter of outer tube (in.)	0.954

**Additions and/or changes for HPWH design model.

**CARD #16		FORMAT (8F10.4)	
	QAC	water mass flow rate (lb_m/h)	681.44
	TAIIC	entering water temperature (°F)	126.6

DATA FOR CONFIGURATION OPTIONS AND REFRIGERANT LINES:

CARD #17		FORMAT (8I10)	
	MCMPOP	switch for adding compressor can heat loss to air from the outdoor coil =0, compressor can loss not added to outdoor air =1, compressor can loss added to air before crossing the outdoor coil =2, compressor can loss added to air after crossing the outdoor coil	0
	MFANIN	switch for adding heat loss from the indoor fan to air stream, settings are similar to those for MCMPOP	1
	MFANOU	switch for adding heat loss from the outdoor fan to air stream, settings are similar to those for MCMPOP	0
CARD #18		FORMAT (8F10.4)	
	QSUCLN	rate of heat gain in the compressor suction line (Btu/h)	63.8
	QDISLIN	rate of heat loss in the compressor discharge line (Btu/h)	315.22
	QLIQLN	rate of heat loss in the liquid line (Btu/h)	544.57
CARD #19		FORMAT (8F10.4)	
	DLL	inside diameter of the liquid line, condenser to TXV (in.)	0.3190
	XLEQLL	equivalent length of the liquid line, condenser to TXV (ft)	5.667
	DLRVIC	inside diameter of the vapor line between the compressor and the evaporator (in.)	0.4440
	XLRVIC	equivalent length of the vapor line between the compressor and the evaporator (ft)	2.92
	DLRVOC	inside diameter of the vapor line between the compressor and the condenser (in.)	0.319
	XLRVOC	equivalent length of the vapor line between the compressor and the condenser (ft)	2.50
CARD #20		FORMAT (8F10.4)	
	DSLRV	inside diameter of the suction line from the evaporator to the compressor inlet (in.)	0.444
	XLEQLP	equivalent length of the low pressure line from the evaporator to the compressor inlet (ft)	0.0
	DDLRV	inside diameter of the discharge line from the compressor outlet to the condenser (in.)	0.319
	XLEQHP	equivalent length of the high pressure line from the compressor outlet to the condenser (ft)	0.0

**Additions and/or changes for HPWH design model.

Appendix C

SAMPLE INPUT DATA

```
TEST DATA FOR HEAT PUMP WATER HEATER
         1
         1         1       100
         0     15.79
         0      7.00
     42.90    149.45
         2     1.428   3450.00       0.0     0.330
 4.533E-05-9.219E-03-9.168E-05-6.056E-03 1.375E-04 1.151E+00  1.43E+00  20.0E+00
-2.742E-03 3.918E-01 4.301E-02 1.312E+00-6.953E-03 8.350E+01
      68.0     0.541
     525.0     111.9    1000.0       0.0
     1.778       2.0       2.0     0.625      1.00      29.0
       2.0      14.0    0.0045    0.3120    0.2890     128.2     196.0       1.0
    192.00     1.200
     0.565     0.565     0.625     0.625     0.954
    679.80     126.6
         0         1         0
     63.80    315.22    544.57
    0.3190     5.667    0.4440      2.92    0.3190      2.50
    0.4440      0.00    0.3190      0.00
```

Appendix D

SAMPLE OUTPUT

```
**** INPUT DATA *****
      TEST DATA FOR HEAT PUMP WATER HEATER -- 2 DATA 16

      SUMMARY OUTPUT
      COOLING MODE OF OPERATION
      WATER-TO-AIR HEAT PUMP
      REFRIGERANT CHARGE IS NOT SPECIFIED

      COMPRESSOR INLET SUPERHEAT IS SPECIFIED AT   15.79 F

      CONDENSER  EXIT SUBCOOLING IS SPECIFIED AT    7.00 F

      ESTIMATE OF:
        SATURATION TEMPERATURE INTO   COMPRESSOR   42.90 F
        SATURATION TEMPERATURE OUT OF COMPRESSOR  149.45 F

      COMPRESSOR CHARACTERISTICS:
        TOTAL DISPLACEMENT                          1.428 CUBIC INCHES
        GIVEN MOTOR SPEED                        3450.000 RPM

      MAP-BASED COMPRESSOR INPUT:
        POWER CONSUMPTION=     4.533E-05*CONDENSING  TEMPERATURE**2 + -9.219E-03*CONDENSING  TEMPERATURE
                             + -9.168E-05*EVAPORATING TEMPERATURE**2 + -5.056E-03*EVAPORATING TEMPERATURE
                             +  1.375E-04*CONDENSING  TEMPERATURE*EVAPORATING TEMPERATURE +  1.151E 00

        MASS FLOW RATE=        -2.742E-03*CONDENSING  TEMPERATURE**2 +  3.918E-01*CONDENSING  TEMPERATURE
                             +  4.301E-02*EVAPORATING TEMPERATURE**2 +  1.312E 00*EVAPORATING TEMPERATURE
                             + -6.953E-03*CONDENSING  TEMPERATURE*EVAPORATING TEMPERATURE +  8.350E 01

        BASE SUPERHEAT FOR COMPRESSOR MAP          20.000 F
        BASE DISPLACEMENT FOR COMPRESSOR MAP        1.430 CU IN

        SUPERHEAT CORRECTION TERMS (SET IN BLOCK DATA):
          SUCTION GAS HEATING FACTOR                0.330
          VOLUMETRIC EFFICIENCY CORRECTION FACTOR   0.750

        HEAT REJECTED FROM COMPRESSOR SHELL IS 0.330 TIMES THE COMPRESSOR POWER


    INDOOR UNIT: EVAPORATOR
      INLET AIR TEMPERATURE                      68.000 F        RELATIVE HUMIDITY                          0.54100
      AIR FLOW RATE                              525.00 CFM      SPECIFIED FAN POWER                         111.90 WATTS
      ID OF EACH OF 6 EQUIVALENT DUCTS          1000.00 IN       HOUSE LOAD TO BE MET BY INDOOR UNIT           0.0 BTU/H
      FRONTAL AREA OF HX                          1.778 SQ FT    WAVY FINS
      NUMBER OF TUBES IN DIRECTION OF AIR FLOW    2.00           FIN PITCH                                    14.00 FINS/IN
      NUMBER OF PARALLEL CIRCUITS                 2.00           FIN THICKNESS                             0.00450 IN
      OD OF TUBES IN HX                        0.31200 IN        THERMAL CONDUCTIVITY: FINS                 128.20 BTU/H-FT-F
      ID OF TUBES IN HX                        0.28900 IN        THERMAL CONDUCTIVITY: TUBES                196.00 BTU/H-FT-F
      HORIZONTAL TUBE SPACING                    0.625 IN        FRACTION OF COMPUTED CONTACT CONDUCTANCE    1.000
      VERTICAL TUBE SPACING                      1.000 IN        NUMBER OF RETURN BENDS                      29.00

    CONDENSER IS WATER TO REFRIGERANT

    TUBE-IN-TUBE HEAT EXCHANGER PARAMETERS
      MODEL NUMBER                                100
      TOTAL LENGTH                             192.00 IN
      OUTSIDE DIAMETER                          0.954 IN
      HEAT TRANSFER ENHANCEMENT FACTOR          1.200
      ENTERING SOURCE TEMPERATURE              126.60 F
      INSIDE DIAMETER                           0.555 IN
      BRINE FLOW (LBS/HR)                      679.80

    POWER TO THE INDOOR  FAN ADDED TO AIR BEFORE CROSSING THE INDOOR  COIL.

    HEAT GAIN IN SUCTION LINE                    63.8 BTU/H
    HEAT LOSS IN DISCHARGE LINE                 315.2 BTU/H
    HEAT LOSS IN LIQUID LINE                    544.6 BTU/H

    DESCRIPTION OF CONNECTING TUBING:
      LIQUID LINE FROM INDOOR TO OUTDOOR HEAT EXCHANGER
          ID                        0.31900 IN
          EQUIVALENT LENGTH            5.67 FT
      FROM INDOOR COIL TO REVERSING VALVE          FROM OUTDOOR COIL TO REVERSING VALVE
          ID                        0.44400 IN           ID                        0.31900 IN
          EQUIVALENT LENGTH            2.92 FT           EQUIVALENT LENGTH            2.50 FT
      FROM REVERSING VALVE TO COMPRESSOR INLET     FROM REVERSING VALVE TO COMPRESSOR OUTLET
          ID                        0.44400 IN           ID                        0.31900 IN
          EQUIVALENT LENGTH            0.0  FT           EQUIVALENT LENGTH            0.0  FT

ITERATION TOLERANCES:
    AMBCON   0.200 F     CMPCON   0.050 BTU/LBM     TOLH     0.00100 BTU/LBM
    CNDCON   0.200 F     FLOCON   0.400 LBM/H       TOLS     0.00005 BTU/LBM-R
    EVPCON   0.500 F     CONMST   0.003 F
```

***** CALCULATED HEAT PUMP PERFORMANCE *****

SYSTEM SUMMARY	REFRIGERANT TEMPERATURE	SATURATION TEMPERATURE	REFRIGERANT ENTHALPY	REFRIGERANT QUALITY	REFRIGERANT PRESSURE	AIR TEMPERATURE
COMPRESSOR SUCTION LINE INLET	53.200 F	39.967 F	83.500 BTU/LBM	1.0000	51.637 PSIA	
SHELL INLET	55.538	39.748	83.897	1.0000	51.437	
SHELL OUTLET	200.293	149.199	101.099	1.0000	246.941	
CONDENSER INLET	190.303 F	149.116 F	99.136 BTU/LBM	1.0000	246.722 PSIA	126.600 F
OUTLET	141.846	148.637	41.638	0.0	245.477	139.927
EXPANSION DEVICE	128.913 F	148.664 F	38.248 BTU/LBM	0.0	245.422 PSIA	
EVAPORATOR INLET	45.762 F	45.752 F	38.248 BTU/LBM	0.3103	57.118 PSIA	68.000 F
OUTLET	53.200	39.967	83.500	1.0000	51.637	56.505

COMPRESSOR PERFORMANCE

COMPRESSOR MOTOR POWER	1.208 KW	EFFICIENCY	
REFRIGERANT MASS FLOW RATE	160.652 LBM/H	OVERALL ISENTROPIC	0.4912
MOTOR SPEED	3450.000 RPM	VOLUMETRIC	0.7622
		AT PRESSURE RATIO OF	4.8009
COMPRESSOR SHELL HEAT LOSS	1361.091 BTU/H	SUPERHEAT CORRECTION TERMS	
		POWER	0.9965
		MASS FLOW RATE	1.0068

WATER PUMP SUMMARY -

FLOW RATE	1.38 GPM	682.4 LBM/HR
POWER	57.0 WATTS	194.5 BTU/HR
HEAD PRESSURE:		
CONDENSER	0.46 FT H2O	0.20 PSIA
EXTERNAL	8.84	3.77
---	---	---
TOTAL	9.30 FT H2O	3.97 PSIA

CONDENSER IS WATER TO REFRIGERANT

TOTAL HEAT TRANSFER	9237. BTU/HR
REFRIGERANT PRESSURE DROP	1.245 PSI
WATER INLET TEMPERATURE	126.60 F
WATER OUTLET TEMPERATURE	139.93 F

FLOW CONTROL DEVICE - CONDENSER SUBCOOLING IS SPECIFIED AS 7.000 F

CORRESPONDING TXV RATING PARAMETERS:		CORRESPONDING CAPILLARY TUBE PARAMETERS:		CORRESPONDING ORIFICE PARAMETER:	
RATED OPERATING SUPERHEAT	11.000 F	NUMBER OF CAPILLARY TUBES	1	ORIFICE DIAMETER	0.0381 IN
STATIC SUPERHEAT RATING	6.000 F	CAPILLARY TUBE FLOW FACTOR	1.317		
PERMANENT BLEED FACTOR	1.150				
FRACTION OF RATED OPENING	1.330				
TXV CAPACITY RATING: WITH NOZZLE AND TUBES	0.272 TONS				

```
PERFORMANCE OF EACH CIRCUIT IN THE EVAPORATOR
        INLET AIR TEMPERATURE                68.000 F
          HEAT LOSS FROM FAN                  381.9 BTU/H
        AIR TEMPERATURE ENTERING COIL        68.661 F
        OUTLET AIR TEMPERATURE               56.505 F

        MOISTURE REMOVAL OCCURS

        SUMMARY OF DEHUMIDIFICATION PERFORMANCE (TWO-PHASE REGION)

                            LEADING EDGE          POINT WHERE MOISTURE                          LEAVING EDGE OF COIL
                              OF COIL                REMOVAL BEGINS
                                AIR              AIR              WALL                AIR                WALL
        DRY BULB TEMPERATURE   68.661 F          58.858 F         50.804 F            55.505 F           49.717 F
        HUMIDITY RATIO        0.00786          0.00786          0.00786            0.00775            0.00755
        ENTHALPY               25.089 BTU/LBM   22.698 BTU/LBM   20.733 BTU/LBM     21.759 BTU/LBM     20.127 BTU/LBM

        RATE OF MOISTURE REMOVAL                                                    0.1164 LBM/H
        FRACTION OF EVAPORATOR THAT IS WET                                          0.3291
        LATENT HEAT TRANSFER RATE IN TWO-PHASE REGION                                 124. BTU/H
        SENSIBLE HEAT TRANSFER RATE IN TWO-PHASE REGION                              3349. BTU/H
        SENSIBLE TO TOTAL HEAT TRANSFER RATIO FOR TWO-PHASE REGION                  0.9642

        OVERALL SENSIBLE TO TOTAL HEAT TRANSFER RATIO                               0.9658

        OVERALL CONDITIONS ACROSS COIL
                                ENTERING        EXITING
                                  AIR             AIR
        DRY BULB TEMPERATURE     68.661 F        56.505 F
        WET BULB TEMPERATURE     57.966 F        53.040 F
        RELATIVE HUMIDITY         0.529           0.802
        HUMIDITY RATIO          0.00786         0.00776

        TOTAL HEAT EXCHANGER EFFECTIVENESS (SENSIBLE)    0.5109

                                          SUPERHEATED        TWO-PHASE
                                            REGION             REGION
        NTU                                 0.6750             0.7221
        HEAT EXCHANGER EFFECTIVENESS        0.4510             0.5142
        CR/CA                               0.3740
        FRACTION OF HEAT EXCHANGER          0.1189             0.8811
        HEAT TRANSFER RATE                   163.2 BTU/H       3473.1 BTU/H
        AIR MASS FLOW RATE                  140.85 LBM/H      1043.61 LBM/H
        OUTLET AIR TEMPERATURE              63.911 F           55.505 F

        AIR SIDE:                                              REFRIGERANT SIDE:
          MASS FLOW RATE                1184.5 LBM/H             MASS FLOW RATE                  80.3 LBM/H
          PRESSURE DROP                  0.162 IN H2O            PRESSURE DROP                  5.481 PSI
          HEAT TRANSFER COEFFICIENT                              HEAT TRANSFER COEFFICIENT
            DRY COIL                   14.162 BTU/H-SQ FT-F       VAPOR REGION                62.136 BTU/H-SQ FT-F
            WET COIL                   15.747 BTU/H-SQ FT-F       TWO PHASE REGION           589.171 BTU/H-SQ FT-F

        CONTACT INTERFACE:
          CONTACT CONDUCTANCE         924.898 BTU/H-SQ FT-F

        DRY FIN EFFICIENCY              0.794
        WET FIN EFFICIENCY (AVERAGE)    0.773
        WET CONTACT FACTOR (AVERAGE)    1.165

        UA VALUES PER CIRCUIT:VAPOR        TWO PHASE
                              REGION        REGION
          REFRIGERANT SIDE    11.928         837.989 BTU/H-F
          AIR SIDE
            DRY COIL          38.445         191.105 BTU/H-F
            WET COIL                          96.392 BTU/H-F
          CONTACT INTERFACE
            DRY COIL         183.199         910.669 BTU/H-F
            WET COIL                        516.651 BTU/H-F
          COMBINED
            DRY COIL           8.672         123.312 BTU/H-F
            WET COIL                          62.751 BTU/H-F


SUMMARY OF ENERGY INPUT AND OUTPUT:
        TEST DATA FOR HEAT PUMP WATER HEATER -- @ DATA 16

        POWER CONSUMPTION:                                   HEAT LOSSES                          HEAT GAIN
          COMPRESSOR        1208.5 WATTS     4124.5 BTU/HR     COMPRESSOR SHELL 1361.1 BTU/HR       SUCTION LINE  63.8 BTU/HR
          FAN                111.9           381.9             DISCHARGE LINE     315.2
          PUMP                57.0           194.5             LIQUID LINE        544.6
          --------------- ------------     -------------
          TOTAL             1377.4 WATTS     4701.0 BTU/HR

        HEAT EXCHANGER CAPACITIES
          CONDENSER         9237.3 BTU/HR
          EVAPORATOR        7272.7

        WATER HEATING PERFORMANCE:
          COP                1.965
          CAPACITY          9237.3 BTU/HR

IHC002I STOP      0
```

Appendix E

LISTING OF CIRCULATING WATER PUMP ROUTINE

```
      FUNCTION XMW(XMW1)
C
      COMMON / TEMP / WTIN, XMU, RHO
C
      COMMON / GEOM / XLHX, DHX, XLEXT, DEXT, EHX, EEXT
C
      COMMON / OUT / XMWFIT, WATTS,  HLHX, HLEXT, HLTOT,
     &               HLHXPS, HLEXPS, HTCTPS, PTITLE(4)
C
C     THIS FUNCTION USED IN CONJUNCTION WITH FUNCTION ZERO BALANCES
C     THE WATER FLOW RATE OF THE CIRCULATING WATER PUMP TO THE
C     WATER-SIDE HEAD PRESSURE OF A HEAT PUMP WATER HEATER.
C
C     INPUT DATA:
C             WTIN    INLET WATER TEMPERATURE (F)
C             XLHX    LENGTH OF THE WATER-TO-REFRIGERANT HEAT EXCHANGER (FT)
C             DHX     INSIDE DIAMETER OF THE INNER TUBE OF THE WATER-TO-
C                     REFRIGERANT HEAT EXCHANGER (FT)
C             EHX     SURFACE ROUGHNESS OF WATER-TO-REFRIGERANT HEAT
C                     EXCHANGER (FT)
C             XLEXT   EQUIVALENT LENGTH OF THE PIPING EXTERNAL TO THE
C                     HEAT EXCHANGER (L/D)
C             DEXT    INSIDE DIAMETER OF THE PIPING EXTERNAL TO THE
C                     HEAT EXCHANGER (FT)
C             EEXT    SURFACE ROUGHNESS OF THE PIPING EXTERNAL TO
C                     THE HEAT EXCHANGER (FT)
C             XMW1    AN ESTIMATE OF THE WATER FLOW RATE (GPM)
C
C     OUTPUT DATA:
C             XMWFIT  THE WATER FLOW RATE (GPM)
C             WATTS   THE PUMPING POWER (WATTS)
C
C     NOTE:
C       -HX REFERS TO THE WATER-TO-REFRIGERANT HEAT EXCHANGER
C       -EXT REFERS TO THE PIPING EXTERNAL TO THE HEAT EXCHANGER
C
C     VISCOSITY OF WATER:
C     THIS IS A FIT TO DATA GIVEN IN MCQUISTON'S AND PARKER'S
C     BOOK, 1977, FOR WATER BETWEEN 60 AND 160 F (LBM/FT-HR).
C
      XMUW(T) = 221.45 * (T**(-1.076))
C
C     DENSITY OF WATER:
C     THIS IS A FIT TO DATA GIVEN IN THE HANDBOOK OF CHEMISTRY
C     AND PHYSICS, 39TH EDITION, FOR THE WEIGHT DENSITY
C     OF WATER BETWEEN 60 AND 160 F (LB/CU FT).
C
      RHOW(T) = 63.205 - 0.0137*T
C
C     CAPACITY OF THE CIRCULATING WATER PUMP:
C     THIS IS A FIT TO THE MANUFACTURER'S DATA (GPM).
C
      XMWF(DP) = (-18.101*DP*DP+265.53*DP-820.68)/60.
C
C     POWER CONSUMPTION OF THE CIRCULATING WATER PUMP:
C     THIS IS A FIT TO THE MANUFACTURER'S DATA (WATTS).
C
      W(DP) = 57.0
C
      XMU = XMUW(WTIN)
      RHO = RHOW(WTIN)
C
C     REYNOLD'S NUMBER OF THE WATER.
C
      REHX = (RHO * 60./7.48) * 4.0 * XMW1 / (3.14159*DHX*XMU)
      CALL FRICT(REHX, EHX, DHX, FHX)
      REEXT = (RHO * 60./7.48) * 4.0 * XMW1 / (3.14159*DEXT*XMU)
      CALL FRICT(REEXT, EEXT, DEXT, FEXT)
```

```
C
C       WATER VELOCITY  (FT/SEC).
C
        VHX = (XMW1/7.48/60.) / (3.14159*DHX*DHX/4.)
        VEXT = (XMW1/7.48/60.) / (3.14159*DEXT*DEXT/4.)
C
C       PRESSURE DROP OF WATER (FT OF WATER).
C
        HLHX = 4.*(FHX*XLHX/DHX * VHX*VHX)/(2.*32.174)
        HLEXT = 4*(FEXT*XLEXT*VEXT*VEXT)/(2.*32.174)
C
C       ADD IN PRESSURE DROP IN WATER LINE DUE TO FLOWMETER (FT OF WATER).
C
        HLEXT = HLEXT+6.686
C
C       TOTAL PRESSURE DROP OF WATER IN SYSTEM (FT OF WATER).
C
        HLTOT = HLHX + HLEXT
C
C       CONVERT PRESSURE DROP FROM FT OF WATER TO PSI.
C
        HLHXPS = HLHX *RHO/144.
        HLEXPS = HLEXT*RHO/144.
        HTOTPS = HLTOT*RHO/144.
C
        XMWFIT = XMWF(HLTOT)
        XMW = XMW1 - XMWFIT
        WATTS = W(HLTOT)
        RETURN
        END
```

INTERNAL DISTRIBUTION

1. V. D. Baxter
2. F. D. Boercker
3. R. S. Carlsmith
4. F. C. Chen
5. F. A. Creswick
6. N. Domingo
7. S. K. Fischer
8. W. Fulkerson
9. M. S. Guy
10. M. Hubbard
11. W. R. Huntley
12. W. L. Jackson
13. L. Jung
14. M. A. Kuliasha
15. W. P. Levins
16. J. M. MacDonald
17. J. F. Martin
18. F. C. Maienschein
19. S. H. McConathy
20. H. A. McLain
21. V. C. Mei
22. J. W. Michel
23. W. R. Mixon
24. C. K. Rice
25. R. B. Shelton
26. M. P. Stulberg
27. G. P. Zimmerman

28–48. K. H. Zimmerman

49–50. Central Research Library

51. Document Reference Section
52. Laboratory Records (RC)

53–54. Laboratory Records Department

55. ORNL Patent Section

EXTERNAL DISTRIBUTION

56. Advanced Mechanical Technology, Inc., 141 California Street, Library, Newton, MA 02158
57. G. C. Aldous, Director of New Products Development, Still-Man Manufacturing, 1011 Volunteer Drive, Box 789, Cookeville, TN 38501
58. Roger Aldrich, The Duo-Therm Corporation, 509 South Poplar Street, La Grange, IN 46761-2399
59. G. Alefeld, Physik-Department der TU Munchen, D-8046 Munchen-Garchin, Federal Republic of Germany
60. Albert E. Allen, Director of Facilities, Food Circus Supermarket, 835 Highway 35, Middleton, NJ 07748
61. R. W. Allen, University of Maryland, Mechanical Engineering Dept., College Park, MD 20742
62. Lawrence Ambs, Department of Mechanical Engineering, University of Massachusetts, Amherst, MA 01003
63. Henry Amistadi, Enercomp, P.O. Box 836, Montpelier, VT 05602
64. John Andrews, Solar Technology Group, Building 701, Brookhaven National Laboratory, Upton, NY 11973
65. Carmen Anzalone, Fedders Corporation, 415 Wabash Avenue, Effingham, IL 62401
66. Roland A. Ares, Hussmann Refrigeration Company, 12999 St. Charles Rock Road, Bridgeton, MO 63044
67. Wong Fun Ark, 15 Jackie Drive, Hackettstown, NJ 07840
68. Theodore Atwood, Senior Research Engineer, Buffalo Research Laboratory, Allied Chemical Corp., 20 Peabody Street, Buffalo, NY 14210

69. C. Douglas Auburg, U.S. Department of Energy, Bonneville Power Admin., P.O. Box 3621, 1002 N. E. Holladay, Portland, OR 97208
70. Jim Augustyn, Berkeley Solar Group, 3140 Grove Street, Berkeley, CA 94703
71. W. Aung, Director, Heat Transfer Program, MEAM, National Science Foundation, Washington, DC 20550
72. James Bard, Bard Manufacturing Co., Inc., P.O. Box 607 Bryan, OH 43506
73. Howard Barkley, Duo-Therm, Division of Motor Wheel Corp., 509 S. Poplar Street, LaGrange, IN 46761
74. Hamp Barnett, Energy Demonstration & Technology, Tennessee Valley Authority, 109 UBB, Chattanooga, TN 37401
75. Greg Barrow, General Maintenance & Construction Manager, First Natl. Supermarkets, Inc., 17000 Rockside Road, Cleveland, OH 44137
76. E. K. Bastress, Energy Conversion & Utilization Technology Div., CS-142, Forrestal Building U.S. Department of Energy, Washington, DC 20585
77. Fred W. Bawel, Preway, 810 E. Franklin Street, P.O. Box 534, Evansville, IN 47704
78. J. Berghmans, Katholieke Universiteit, Institut Mechanica, Celestijnenlaan 300 A, B-3030 Heverlee-Belgium
79. A. E. Bergles, Department of Mechanical Engineering, Iowa State University, Ames, IA 50011
80. Morton Blatt, Electric Power Research Institute, Post Office Box 10412, Palo Alto, CA 94303
81. J. H. Bley, Salt River Project, Box 1980, Phoenix, Arizona 85001
82. Peter Bodett, Duo-Therm Division, Goodyear Tire & Rubber Co., 509 S. Poplar Street LaGrange, IN 46761
83. Charles A. Bomely, Jr., Sweet Life Foods, Suffield Distribution Center, P.O. Box 385, Windsor Locks, CT 06096
84. Ulrich Bonne, Honeywell Incorporated, 10701 Lyndale Avenue South, Corporate Technology Center, Materials & Processes Dept., Bloomington, MN 55420
85. James E. Bose, School of Technology, Oklahoma State University, Stillwater, OK 74078
86. Dennis Bossi, V-P, Systems & Services, Fisher Foods, Inc., 5300 Richmond Road, Bedford Heights, OH 44146
87. Jean Boulin, Department of Energy, CE-111.1, FORSTL, Washington, D.C. 20585
88. Richard C. Bozarth, Reco Ind. Inc., P.O. Box 25189, Richmond, VA 23260
89. Gene Brewer, National Institute of Building Sciences, 1015 Fifteenth Street, N.W., Suite 700, Washington, DC 20005
90. Daniel J. Brimm, President, Chem-tronics, Inc., P.O. Box 1604, El Cajon, CA 92022
91. R. A. Brown, United Illuminating, 1115 Broad Street Bridgeport, Connecticut 06609
92. Ralph Bryant, Development Engineer, 635 Thompson Lane, P.O. Box 40566, Heil Quaker Corp., Nashville, TN 37204
93. Donald Burk, Engineering Manager, Albertson's, Inc., P.O. Box 20, 250 Parkcenter Blvd., Boise, ID 83726
94. J. Cairns, Robert University of Michigan Dearborn, School of Engineering, Dept. of Mech. Eng., Dearborn, MI 48128

95. James M. Calm, Project Manager, Heat Pump Development, Electric Power Research Institute, Post Office Box 10412, Palo Alto, CA 94303
96. Gilbert Carlson, ITT Fluid Handling Division, 4711 Golf Road, Skokie, IL 60076
97. C. Gerald Carrington, Department of Physics, University of Otego, Dunedin, New Zealand
98. Mark Catan, Building 701, Brookhaven National Laboratory, Upton, NY 11973
99. Paul E. Chaney, Texas Electrical Service, P.O. Box 970, Ft. Worth, TX 76101
100. Bart Chezar, New York State Power Authority, 10 Columbus Circle New York, New York 10019
101. Cheng-C. Chi, 14905 Chestnut Ridge Court, Gaithersburg, MD 20878
102. Henry M. Chorney, 5244 Barron Drive, N.W., Calgary Alta CANADA, T2L 1T6 QA030
103. Larry Ciecior, Omaha Public Power District, 1623 Harney Street, Omaha, NE 68102
104. D. Claridge, Civil, Environmental, & Architectural Eng., University of Colorado, Campus Box 428, Boulder, CO 80303
105. John A. Clark, Jr., 21 Lions Street, E. Stroudsburg, PA 19301
106. Norm Clark, KTT, Office of Conservation, Bonneville Power Adm., Post Office Box 3621, Portland, Oregon 97208
107. Raymond Cohen, Ray Herrick Laboratories, Purdue University West Lafayette, Indiana 47907
108. H. S. Coleman, Acting Deputy Assistant Secretary for Conserv., Department of Energy, CE-10, 1000 Indepedence Avenue, S.W., Washington, D.C. 20585
109. W. R. Coleman, Residential & Commercial Services, American Electric Power Services, 180 East Broad, Columbus, OH 43201
110. Denver Collins, State Industries, Product Engineering, Cumberland Street, Ashland City, TN 37015
111. David Colvin, Triangle R & D Corporation, P.O. Box 12696, Research Triangle Park, NC 27709
112. Congressional Information Service, Research Building 83, Kodak Park, Rochester, NY 14050
113. R. F. Connor, Whirlpool Corporation, U. S. Highway 41N Evansville, IN 47727
114. Robert E. Cook, 1435 Budd Boulevard, Kankakee, IL 60901
115. W. D. Cooper, Refrigerants & Blowing Agents Freon Products Laboratory, E. I. DuPont de Nemours & Co., Wilmington, DL 19898
116. W. Counihan, 16 Newberry Avenue, Staten Island, New York 10304
117. Steve Crest, Mountain Fuel Supply Company, 180 East First South, P.O. Box 11368, Salt Lake City, Utah 84139
118. Kenneth Cuccinelli, Division of Marketing Services, American Gas Association, 1515 Wilson Blvd., Arlington, VA 22209
119. Lee Culpepper, Tennessee Valley Authority, 330 401 Building, Chattanooga, TN 37401
120. James G. Crawford, Trane CAC, Inc., 6200 Troup Highway, Tyler, TX 75711
121. P. G. Daugirda, Rheem Manufacturing Company, 7600 S. Kedzie, Chicago, IL 60652
122. Kenneth J. Davies, Johnson & Starley, Rhosili Road, Brackmills, Northhampton NN4 OLZ, England N3013
123. Robert DeHaan, Chief Engineer, Heating & Cooling Products, Amana Refrigeration, Inc., Amana, IA 52204

124. Gerry DeMoff, Energy Manager, Chatham Supermarkets, Inc., 2300 E. Ten Mile Road, Warren, MI 48091
125. Gerald Dennahy, Brookhaven National Laboratory, Building 120, Upton, NY 11973
126. Irvin Derks, Manager Engineering Development, Bard Manufacturing Co., P.O. Box 607, Bryan, OH 43506
127. Douglas DeWerth, Project Manager, Utilization Technology, American Gas Association, Research & Development, 8501 E. Pleasant Valley Rd., Cleveland, OH 44131
128. J. Brian Dietz, Vice President, Lone Star Gas Company, 301 South Harwood Street, Dallas, TX 75201
129. Bill Dittman, Copeland Corporation, 1675 W. Campbell Road, Sydney, OH 45365
130. Bill Dollars, Engineering & Research, ARCO Comfort Products Co., 302 Nichols Drive, Hutchins, Texas 75141
131. J. J. Donnelly, Mobil Research & Development Corp., Paulsboro Laboratory, Paulsboro, New Jersey 08066
132. Charles E. Dorgan, Director, Engineering Tech. Center, University of Wisconsin, Ext. 825 Ext. Building, 432 N. Lake Street, Madison, WI 53706
133. Richard Dougall, Dept. of Mechanical Engineering, University of Pittsburgh, Pittsburgh, PA 15261
134. J. Pat Dougherty, Senior Project Engineer, InterNorth, Energy Evaluation & Res. Div., 2223 Dodge Street, Omaha, NE 68102
135. L. N. Dufrene, Central Louisiana Electric Co., Post Office Box 510, Pineville, Louisiana 71360
136. P. O. Dumont, Ateliers De Constructions, Electriques De Charleroi, Groupe Thermo-Mecanique et Nucleaire B-6000, Charleroi, Belgium
137. Robert Dunning, EUS, 201 Seco Road, Monroeville, PA 15146
138. Alex Dybbs, Case Western Reserve University, Glennan Building, Cleveland, OH 44106
139. Amir Ecker, Pyradyne, Inc., 302 Nichols Drive, Hutchins, TX 75141
140. Edison Electric Institute, 8th Floor, 1111 19th Street N.W. Washington, DC 20036
141. Editors, Fine Homebuilding Magazine, Post Office Box 355, Newtown, Connecticut 06470
142. A. H. Elmahdy, Energy and Services Section, National Research Council, Division of Building Research, Ottawa, Canada K1A OR6
143. Energy Conservation Distribution, Oak Ridge National Laboratory, Building 9102-2, Oak Ridge, TN 37830
144. Richard English, Research Division, Carrier Corporation, Carrier Parkway, P.O. Box 4808, Syracuse, NY 13221
145. Raul Esparza, Daikin Air Conditioning America, Inc., 1754 Technology Drive, Suite 116, San Jose, CA 95110
146. J. N. Eustis, Department of Energy, Office of Industrial Programs, CE-121.1, 1000 Independence Avenue, S.W., Washington, DC 20585
147. Phillip D. Fairchild, Electric Power Research Institute, Post Office Box 10412, Palo Alto, California 94303
148. Scott Farley, Heating & A.C. Group, The Coleman Company, Inc., 3110 North Mead, Wichita, KS 67201

149. Mark Felpausch, Director of Store Engineering, Felpausch Food Centers, 127 S. Michigan Avenue, P.O. Box 160, Hastings, MI 49508
150. Harry Fischer, P. O. Box 445, Maggie Valley, NC 28751
151. Robert D. Fischer, Battelle-Columbus Laboratory, 505 King Avenue, Columbus, OH 43201
152. Douglas Fisher, General Electric Co., Major Appliance Business Group, AP1-210, Louisville, KY 40225
153. R. J. Fiskum, Energy Conversion Equipment Branch, CE-112, GF-217/FORS, 1000 Independence Avenue S.W., Washington, DC 20585
154. Eben V. Fodor, Energy Systems Eng., American Gas Association, 1515 Wilson Blvd., Arlington, VA 22209
155. Jeff Forker, Editor-In-Chief, Contracting Business, 1111 Chester Avenue, Cleveland, OH 44114
156. Gilbert M. Freedman, Energy Management Engineer, Alleghany Electric Corporation, Post Office Box 1266, Harrisburg, PA 17108-1266
157. Al Fritsch, Appalachia Sci. in the Pub. Interest, P.O. Box 298, Livingston, Kentucky 40445
158. K. E. Fuller, New York State Electric & Gas Corporation, 4425 Old Vestal Road, Binghamton, New York 13902
159. Steve Galanter, Southern Cal. Edison, P.O. Box 5080, Covina, CA 91723
160. Hernando Galvis, Southern Union Gas, First International Bldg., Dallas, TX 75270
161. Don P. Gatley, Gatley & Associates, 489 Westover Drive, NW, Atlanta, GA 30305
162. Howard Geller, Institute for Local Self Reliance, 1717 18th Street, N.W., Washington, DC 20009
163. John Genung, Coordinator, New Homes Program, Tennessee Valley Authority, 1719 West End Building, Nashville, Tennessee 37203
164. Ted Gilles, Lennox Industries, Inc., Promenade Towers, P.O. Box 400450, Dallas, TX 75240
165. P. V. Gilli, Graz University of Technology, Kopernikusgasse 24, A-8010, Graz, Austria
166. S. Malcolm Gillis, Professor, Public Policy and Economics, Duke University, 4875 Duke Station, Durham, North Carolina 27706
167. Paul Glamm, The Trane Company, 3600 Pammell Creek Road, LaCrosse, WI 54601
168. L. R. Glicksman, Massachusetts Institute of Technology, 77 Massachusetts Bldg. 3-137, Cambridge, MA 02139
169. Earl J. Gmoser, Electrical Testing Laboratories, Inc., Industrial Park, Cortland, NY 13045
170. John C. Goldsmith, U.S. Department of Energy, 1000 Independence Avenue, S.W., CE 311.1, Rm 5H065, Washington, DC 20585
171. Jack Goodman, Science Applications, Inc., 1257 Tasman Drive, Sunnyvale, CA 94806
172. D. N. Granberg, Manager, Energy System Lab., A. D. Smith Corporation, 3533 N. 27th Street, Milwaukee, WI 53216
173. E. Granryd, Dept. of Applied Thermodynamics and Refrigeration, Royal Institute of Technology, S-10044 Stockholm, Sweden
174. Richard Greenhaus, Consumer Reports, 256 Washington Street, Mt. Vernon, NY 10550

175. Cray Griffith, Naval Oceangraphic Office, Code 0010, NSTL Station, Bay St. Louis, MI 39522
176. James E. Griffith, Research & Technical Lab., PSE&G Research Corporation, 200 Boyden Avenue, Maplewood, NJ 07040
177. Marvin E. Gunn, Jr., Energy Conversion & Utilization Technology Div., CS-142, SE-091/FORS, U.S. Department of Energy, 1000 Independence Ave., SW, Washington, DC 20585
178. Tom Gutmann, U.S. Department of Energy, Mailstop CE-113, 1000 Independence Avenue, Washington, DC 20585
179. John Hackstedde, Tecumseh Products Company, Tecumseh, MI 49286
180. Allen J. Hanley, 79 Arlington Avenue, Montreal P. Q. CANADA, H3Y 2W5 QQ310
181. Charles Harmkie, Agency Approvals Engineer, The Singer Company, Controls Division, 9655 West Soreng Avenue, Schiller Park, Illinois 60176
182. James R. Harnish, Unitary Products Engineering, York Div., Borg-Warner Corp., P.O. Box 1592, York, PA 17405
183. James Harris, National Bureau of Standards, Building 202, Room 149, Gaithersburg, MD 20899
184. David T. Harrje, CEES, Engineering Quad, Princeton University, Princeton, NJ 08544
185. P. C. Hastings, Central Maine Power Company, Edison Drive, Augusta, Maine 04336
186. Michael E. Heidenreich, Director of Engineering, Home Div. of Lear Siegler, 900 Brooks Avenue, Holland, MI 49423
187. Gene Heileman, Whirlpool Corporation, Research and Engineering Building, Monte Road, Benton Harbor, MI 49022
188. J. D. Helms, Jr., Tennessee Valley Authority, Applachian District, Office of Power 200 BVB, Knoxville, Tennessee 37902
189. Richard J. Hembach, Conversion & Resources, Consolidated Edison Co., 4 Irving Place, New York, NY 10003
190. Bryan Hibbard, Director, Maintenance & Construction, Eberhard Foods, 4001 West 3 Mile Road, Grand Rapids, MI 49504
191. James Hill, National Bureau of Standards, Building 226, Room B306, Gaithersburg, MD 20899
192. Carl C. Hiller, Electric Power Research Institute, 3412 Hillview Avenue, Palo Alto, CA 94303
193. Keith Hollingsworth, N. C. Alternative Energy Corporation, P. O. Box 12699, Research Triangle Pk., NC 27709
194. Norman Hughes, Conservation & Renewable Energy, 1000 Independence Ave., CE-5, Room 6C036, Washington, DC 20585
195. Leonard Hull, Indianapolis Power & Light, 25 Monument Circle, P.O. Box 1595B, Indianapolis, IN 46206
196. Bao Hwang, David Taylor Naval Ship R&D Center, Mail Code 2722, Annapolis Annapolis Laboratory, Annapolis, MD 21402
197. Fayez F. Ibrahim, Vice-President of R&D, Tyler Refr. Corp., 1329 Lake Street, Niles, MI 49120
198. Institute for Energy Analysis, ORAU-Library
199. Howard Izawa, InterNorth, Inc., 2223 Dodge Street, Omaha, NE 68102

200. Heintz Jaster, Corporate Research & Development, General Electric Company, P. O. Box 43, Schenectady, NY 12345
201. Larry L. Jenkins, Professional Engineering Company, 2211 North 91st Court, Omaha, NE 68134
202. C. W. Jennings, Tennessee Valley Authority, 375 401 Building, Chattanooga, TN 37401
203. O. David Johnson, Residential Appliances, Gas Research Institute, 8600 W. Bryn Mawr Avenue, Chicago, IL 60631
204. Dean Joiner, Fisher & Paykel, Ltd., Refrigerator Division, P.O. Box 58-046, East Tamaki, Auckland, New Zealand
205. Robert Jones, Product Manager, A. O. Smith Corp., P.O. Box 28, Kankakee, IL 60901
206. P. Joyner, The Trane Company, 3600 Pammel Creek Road, LaCrosse, WI 54601
207. Fritz R. Kalhammer, Energy Management and Utilization Division, Electric Power Research Inst., 3412 Hillview Avenue, P.O. Box 10412, Palo Alto, CA 94303
208. F. Kalivoda, Copeland Corporation, 1675 W. Campbell Road, Sydney, OH 45365
209. Theodore Kapus, Building Equipment Division, Department of Energy, CE-112, Room GF-217/FORS, 1000 Independence Avenue, S.W., Washington, DC 20585
210. Roger E. Kasperson, Professor of Government and Geograhy, Gradute School of Geography, Clark University, Worcester, Massachusetts 01610
211. Herbert Kaufman, ARCO Comfort Products Company, 1271 Avenue of the Americas, New York, NY 10020
212. Ken Kazmer, Gas Research Institute, 8600 West Bryn Mawr Avenue, Chicago, IL 60631
213. Richard W. Kelso, University of Tennessee, School of Architecture, 100 Estabrook Hall, Knoxville, TN 37916
214. Rube Kelto, Tecumseh Products Company, 100 E. Patterson St., Tecumseh, MI 49286
215. Robert Kiley, Thermar - The Tankless Heater Corp., Post Office Box 108, Matamores, Pennsylvania 18336
216. R. W. King, Manager, Product Evaluation, Copeland Corporation, 1675 W. Campbell Road, Sydney, OH 45365
217. C. H. Kirk, AMTROL, Inc., 1400 Division Road, W. Warwick, Rhode Island 02893
218. A. J. Kloska, Group Leader, Range/Combustion, Sears, Roebuck and Co., Product Evaluation Lab., 925 S. Holman Avenue, Chicago, IL 60607
219. Paul Kolb, Director R&D, ETL Testing Laboratory, Inc., Industrial Park, Cortland, NY 13045
220. William Kolosi, Ohio Edison Company, 76 South Main, Akron, OH 44308
221. Shigeki Kondoh, Technical Development Center, Mitsui & Co. (USA), Inc., 200 Park Avenue, New York, NY 10166
222. Ira Krepchin, Foster-Miller Associates, Inc., Engineers, 350 Second Avenue, Waltham, MA 02254
223. Thomas Kroeschell, Division Commercial Manager, Commonwealth Edison Company, P.O. Box 278, IN 423 Swift Road, Lombard, IL 60148
224. M. J. Kroninger, Caloric Corporation, Heffner & Washington Streets, Topton, PA 19562
225. H. Kruse, University Hannover, Welfengarten 1 A, 3000 Hannover 1, Federal Republic of Germany

226. Marvin Kushner, Vice-President, Food Fair, Inc., 3490 N.W. 71st Street, Miami, FL 33147
227. E. Kweller, Building Equipment Division, National Bureau of Standards, Building 226, Room B320, Gaithersburg, MD 20899
228. R. J. LaSala, Geothermal and Hydro Power Division, Department of Energy, 1000 Independence Avenue, SW, Washington, DC 20585
229. Z. Lavan, Dept. of Mechanical Engineering, Illinois Inst. of Technology, Chicago, IL 60616
230. Jon Leber, California Energy Commission, MS-25, 1516 Ninth Street, Sacramento, CA 95814
231. W. David Lee, Arthur D. Little, Inc., 32 Acorn Park, Cambridge, MA 02140
232. Y. N. Lee, Roy C. Ingersoll Research Center, Wolf & Algonquin Roads, Borg-Warner Corporation, Des Plaines, IL 60018
233. Martin Lessen, 12 Country Club Drive, Rochester, New York 14618
234. Pete Likes, Vice-President and Director of Res., Hussman Refrigeration, 12999 St. Charles Rock Road, Bridgeton, MO 63044
235. Danny C. Lim, Energy Conversion Equipment Branch, CE-112, Rm. GF-217/FORS, U.S. Department of Energy, 1000 Independence Avenue S.W., Washington, DC 20585
236. Harold Lorsch, Franklin Research Laboratories, Twentieth & Parkway, Philadelphia, PA 19103
237. Nance Lovvorn, Alabama Power Company, P.O. Box 2641, Birmingham, AL 35291
238. Ward MacArthur, Honeywell Inc., 1700 West Highway 36, St. Paul, MN 55113
239. Robert A. Macriss, Institute of Gas Technology, 4201 W. 36th Street, Chicago, IL 60632
240. Hugh Maguire, Cincinnati Gas & Electric, P.O. Box 960, Cincinnati, OH 45201
241. J. C. Major, Swiss Federal Institut for Reactor Research, CH-5303 Wurenlingen, Switzerland
242. Venkata S. Manian, 27409 Hystone Drive, Farmington Hills, MI 48018
243. Mack Mansfield, Houston Lighting and Power Company, Commercial Research, Post Office Box 1700, Houston, Texas 77001
244. R. Marshall, Research & Development Section, 8th Floor, 101 Bloor Street West, Toronto, Ontario M5S 1P8
245. R. Michael Martin, California Energy Commission, Conservation Division, 1516 Ninth Street, Sacramento, CA 95814
246. Michael J. McCabe, Building Equipment Division, Department of Energy, CE-112, Rm. GF-217/FORS, 1000 Independence Avenue, S.W., Washington, D.C. 20585
247. Martin McCall, Project Manager; Research & Development, Consumers' Gas Company Ltd., P.O. Box 650, 500 Consumers Road, Willowdale, Ontario M1K 5E3
248. William A. Messner, Advanced Energy Systems, Consolidated Edison Co., 4 Irving Place, New York, NY 10003
249. Philip Metz, Brookhaven National Laboratory, Building 701, Upton, NY 11973
250. John P. Millhone, Office of Buildings Energy Research & Development, U.S. Department of Energy, CE-11, Rm. GF-231/FORS, 1000 Independence Avenue S.W. Washington, DC 20585

251. Mark Minakuchi, Sharp Electronics Corporation, P.O. Box 588, 10 Keystone Place, Paramus, NJ 07652
252. S. Miyazaki, Senior Product Engineer, Sears Roebuck & Co., Dept. 817, Sears Tower, Chicago, IL 60684
253. H. J. Moore, American Appliance Manufacturing Corp., General Office and Factory, 2341/2425 Michigan Avenue, Santa Monica, CA 90404
254. W. Calvin Moore, 360 Tri-Hill Drive, York, PA 17403
255. Eugene C. Moran, Springfield Operations Office, Washington Gas Light Co., 6801 Industrial Road, Springfield, VA 22151
256. Louise S. Morrison, Solar Energy Research Institute, 1617 Cole Blvd., Golden, CO 80401
257. F. H. Morse, Office of Solar Heat Technologies, U. S. Department of Energy CE-31, 1000 Independence Avenue S.W., Washington, DC 20585
258. Bruce Moyer, Pennsylvania Rural Elec. Assoc., Energy Management Specialist, P.O. Box 1266, 212 Locust Street, Harrisburg, PA 17108
259. William E. Murphy, Department of Mechanical Engineering, Texas A&M University, College Station, TX 77843
260. W. Russell Newton, Tennessee Valley Authority, 205 Sheraton Building, Chattanooga, TN 37401
261. David Nichols, Research Scientist, Energy Systems Research Group, Inc., 120 Milk Street, Boston, Massachusetts 02109
262. Y. Noda, Noda Engineering Corporation, 2-9-14 Matsugaoka, Kugenuma, Fujisawa City, Kanagawa Perfecture, Japan
263. E. A. Nordstrom, Director, Product Engineering, A. O. Smith Corporation, Consumer Products Division, P.O. Box 28
264. Albert Nunez, Solarr King Supply, 15535 New Hampshire Ave., Silver Springs, MD 20904
265. Otto J. Nussbaum, Halstead and Mitchell, P.O. Box 1110, Scottsboro, AL 36768
266. Office of the Assistant Manager for Energy R&D, U.S. Department of Energy, Oak Ridge Operations, Oak Ridge, TN 37830
267. R. E. Oliver, Department of Energy, CE-111.1, FORSTL, Washington, D.C. 20585
268. John O'Malley, Energy Manager Co-Ordinator, Dominick's Finer Foods, Inc., 333 Northwest Avenue, Northlake, IL 60164
269. James W. Osborne, Department of Energy, CE-121, FORSTL, 1000 Independence Avenue, S.W., Washington, D.C. 20585
270. Andrew Paczuski, Principal Engineer, Briston Compressors, Inc., 649 Industrial Park Rd., Bristol, VA 24201
271. Jerald Parker, School of Mechanical & Aerospace Eng., Oklahoma State University, 218 Engineer North, Stillwater, OK 74078
272. David M. Pellish, Department of Energy, CE-312, FORSTL, Washington, D.C. 20585
273. Maier Perlman, Ontario Hydro, Utilization Research Eng., 800 Kipling Avenue, Toronto, Ontario M8Z 5S4
274. George Peterson, Energy Coordination Office, City Hall, Room 334, City of Minneapolis, Minneapolis, MN 55415

275. Hung Pham, Trane DPG, Inc., 6200 Troup Highway, Tyler, TX 75711
276. B. A. Phillips, Phillips Engineering Company, 721 Pleasant Street, St. Joseph, MI 49085
277. Joe Pietsch, 4319 Bobbitt Drive, Dallas, TX 75229
278. T. R. Potter, North Carolina Energy Institute, Energy - NC/STRC, N. C. Dept. of Commerce, P.O. Box 12235, Research Triangle Pk., NC 27709
279. Ralph Powe, Associate Vice President for Research, Mississippi State University, P.O. Drawer G, 617 Allen Hall, Mississippi State, MS 39762
280. R. L. Puterbaugh, Vice President, Consumer Products Engineering, White Consolidated Ind., Inc., 11770 Berea Road, Cleveland, OH 44111
281. Fredercik Puelle, Novatech Resource Corp., 9 West 57th Street, Suite 3750, New York, NY 10019
282. V. Recchi, National Research Council, % O. T. B. Zona Industriale, Contrada del Parco, Bari, Italy
283. K. Regenos, GTE Communication Products, P.O. Box 7188, Mountain View, CA 94047
284. Edward A. Reid, Jr., Columbia Gas Syst. Serv. Corp., 1600 Dublin Road, P.O. Box 2318, Columbus, OH 43216
285. Paul J. Reynolds, Corporate Director of Engineering, First National Supermarkets, 500 North Street, Windsor Locks, CT 06096
286. Joseph Rizzuto, New York State Energy Research & Development Auth., Agency Building No. 2, Rockefeller Plaza, Albany, NY 12223
287. Robert Rogers, Vice-President of Engineering, Americold Compressor Company, 2340 Second Avenue, NW, Cullman, Alabama 35055
288. A. Rojey, Institut Francais du Petrole, 14 Avenue de Bois-Preau, BP 311, Ruei P Malmaison Cedex, France
289. H. Ross, Office of Buildings and Community Systems, Department of Energy, 20 Massachusetts Ave., NW, MS-2221C, Washington, DC 20545
290. J. H. Rothenburg, Utilities Systems, Dept. of Housing & Urban Dev., 451 Seventh Street S.W, Washington, DC 20410
291. Jacques Rouhault, et Developpement Commercial, Direction Marketing, 2 avenue du Vieil Etan, BP 19, VERSAILLES (3) 0438134
292. William Rudoy, University of Pittsburgh, 323 Benedum Engineering Hall, Pittsburgh, PA 15261
293. Ralph Rustebakke, Dairy Equipment Company, Post Office Box 8050, Madison, WI 53708
294. J. D. Ryan, Energy Conversion Equipment Branch, CE-112, GF-217/FORS, U. S. Department of Energy, 1000 Independence Avenue S.W. Washington, DC 20585
295. W. J. Sandle, Department of Physics, University of Otego, Dunedin, New Zealand
296. Maxine Savitz, 5019 Lowell Street, N.W., Washington, DC 20016
297. Dick Schrevier, ACUREX, 485 Clyde Avenue, Mountainview, CA 94042
298. T. C. Scott, Dept. of Mechanical & Aerospace Eng., University of Virginia, Thornton Hall - Eng. School, Charlottesville, VA 22901
299. E. Searight, Thermo Electron Corporation, 101 First Avenue, Waltham, Massachusetts 02154

300. William W. Seaton, ASHRAE, Inc., 1791 Tullie Circle, NE, Atlanta, GA 30329
301. Takao Senshu, Mechanical Engineering Research Laboratory, Hitachi, Ltd., 390 Muramatsu, Shimizu-shi, Shizuoka-ken, Japan
302. Charles Sepsey, Dept. of Mechanical Engineering, Ohio State University, Room 2075 - Robinson Lab, 206 West 18th Avenue, Columbus, OH 43210
303. Mohammed Shah, Consulting Engineer, 15 Rush Street, Port Jefferson Sta., NY 11776
304. Ramesh Shah, Technical Director of Research, Harrison Radiator Division, General Motors Corporation, Lockport, NY 14094
305. James D. Shaw, Public Service Company of Oklahoma, P.O. Box 201, Tulsa, OK 74102
306. D. Sheldon, Oregon Water Heater Company, 4040 International Way, Milwaukie, OR 97222
307. T. Sheldon, Tennessee Valley Authority, 330 401 Building, Chattanooga, TN 37401
308. Samuel V. Shelton, Thermax, Inc., 296 14th St.,NW, Atlanta, GA 30318
309. Yusuf A. Shikari, Project Manager, Gas Research Institute, 8600 West Bryn Mawr Avenue, Chicago, IL 60631
310. Dean Shupe, Dept. of Mech. & Industrial Eng., Mail Location 72, University of Cincinnati, Cincinnati, OH 45221
311. Ken Singh, EMAX, Inc., 2701 Indianola Avenue, Columbus, OH 43202
312. James A. Smith, Test and Evaluation Branch, CE-111, Rm. GF-253/FORS, U.S. Department of Energy, 1000 Independence Avenue S.W. Washington, DC 20585
313. Douglas Solley, Thermodyne, P.O. Box 1007, West Columbia, SC 29169
314. Mason Somerville, Professor, Dept. of Mech. Eng., University of Arkansas, Fayetteville, AR 72701
315. R. Sonderegger, Lawrence Berkeley Laboratory, 90-3074, 1 Cyclotron Road, Berkeley, CA 94720
316. Christian Spaeth, Energy Manager, Bells Markets, 355 Harlem Road, Buffalo, NY 14206
317. Hans Spauchus, Energy and Materials Sciences Lab, Georgia Inst. of Technology, Atlanta, GA 30332
318. Joe M. Spears, Jr., Central Power and Light Co., P.O. Box 2121, Corpus Christi, TX 78403
319. Carl Speich, Staff Engineer-Advanced Development Engineering, The Trane Company, 3600 Pammel Creek Road, LaCrosse, WI 54601
320. Charles Staats, Engineer, Research & Development, Bradford-White Corporation, 24th & Ellsworth Streets, Philadelphia, PA 19146
321. Leo P. Stambaugh, Jr., 6605 Aintree Circle, Dallas, TX 75214
322. Frank Stanonik, GAMA, 1901 North Fort Myer Drive, P.O. Box 9245, Arlington, VA 22209
323. K. E. Starner, Advance Engineering, York Division, Borg-Warner Coporation, P.O. Box 1592, York, PA 17405
324. Robert Steffy, Jr., Director, Div. of Energy Conservation and Rates, Tennessee Valley Authority, 703 Power Building, Chattanooga, TN 37401
325. Lloyd Stenbeck, Vice President - Store Planning & Engineering, Super Valu Stores, Inc., P.O. Box 990, Minneapolis, MN 55440
326. Richard Stepler, Consumer Information Editor, Popular Science, 380 Madison Avenue, New York, NY 10017

327. Studsvik Energiteknik AB, Library, S-611 Nykoping, Sweden
328. Paul Swenson, East Ohio Gas Company, P. O. Box 5759, Cleveland, OH 44101
329. C. J. Swet, 7040 Woodville Road, Mt. Airy, MD 21771
330. W. D. Syniuta, Advanced Mechanical Technology, Inc., 141 California Street Newton, MA 02158
331. Technical Information Center, Department of Energy, P.O. Box 62, Oak Ridge, TN 37831, for Dist. Category UC-95d
332. W. Teich, Raytheon Company, NPC Foundry Avenue, P.O. Box 33, Waltham, MA 02254
333. Marvin Thedford, Jr., Texas Utility Electric Co., 1506 Commerce Street, Dallas, TX 75201
334. W. C. Thomas, Virginia Polytechnic Inst. & State Univ., Mech. Eng. Dept., Blacksburg, VA 24061
335. Seth Thomason, Southwestern Public Service Company, P.O. Box 1261, Amarillo, Texas 79170
336. R. Topping, Arthur D. Little Inc., 32 Acorn Park, Cambridge, MA 02140
337. Hamid Torab, 1837 Shirley Lane, Apartment A3, Ann Arbor, MI 48105
338. William Toscano, Aspen, P.O. Box 809, Sudbury, MA 01776
339. E. L. Tramel, Cons. & Energy Mgmt. Branch, Tennessee Valley Authority, 350-401 Building, Chattanooga, TN 37401
340. W. H. Tucker, Chemical Engineering Dept., Tri-State University, Angola, IN 46703
341. Gunnar Walmet, New York State Energy Research & Development Auth., Two Rockefeller Plaza, Albany, NY 12223
342. Donald Walukas, Gas Research Institute, 8600 W. Bryn Mawr Avenue, Chicago, IL 60631
343. C. Wan, National Bureau of Standards, EM204, NBS, Gaithersburg, MD 20899
344. R. F. Welguisz, Trane CAC, Inc., Suite 212, 4161 Carmichael Avenue, Jacksonville, FL 32207
345. Ernest Wenczl, State Industries, Inc., Ashland City, Tennessee 37015
346. Nancy Wenke, Puget Power, Post Office Box 868, Bellevue, Wash. 98009
347. Alan Werhane, Amana Refrigeration, Inc., Amana, IA 52204
348. J. F. Whitbeck, Idaho National Engineering Laboratory, P.O. Box 1625, Idaho Falls, ID 83401
349. David J. Whitlock, Commercial & Industrial Dept., Rochester Gas & Electric Corp., 89 East Avenue, Rochester, NY 14649
350. Ronald R. Wisner, Manager, Product Engineering, Tecumseh Product Company, 100 E. Patterson Street, Tecumseh, MI 49286
351. M. W. Woodford, Air-Conditioning & Refrigeration Inst., 1501 Wilson Blvd., 6th Floor, Arlington, VA 22209
352. Lawrence Woodwarth, Brookhaven National Laboratory, Building 475, Upton, NY 11973
353. William M. Worek, Illinois Institute of Technology, Dept. of Mechanical Eng., 10 West 32nd Street, Chicago, IL 60616
354. Eugene Wright, Freon Products Laboratory, DuPont Corp., Chestnut Run Site, Wilmington, DL 19898

355. J. Richard Wright, Director of Technology, ASHRAE, Inc., 1791 Tullie Circle, NE, Atlanta, GA 30329
356. Leslie Wright, A. O. Smith Corporation, 12100 West Park Place, P. O. Box 23994, Milwaukee, WI 53223-0994
357. Jerry Wurm, Institute of Gas Technology, 3424 South State Street, IIT Center, Chicago, IL 60616
358. Marvin Yarosh, Associate Director, Florida Solar Energy Center, 300 State Road 401, Cape Canaveral, FL 32920
359. T. Yoshii, Assistant Manager (Technical Investigation), Mitsubishi Heavy Industries, A.C. & Refrigerating Machinery, Tokyo 108 Japan
360. David Young, Ontario Hydro, Research Division, 800 Kipling Avenue, Toronto, Canada M8Z 5S4
361. Joe Zaccaria, Advisory Director, Emerson Quite Kool, 400 Woodbine Avenue, Woodbridge, New Jersey 07095
362. Gordon Zahn, Manager, Corp. Energy Conservation, H. E. Butt Grocery Co., P.O. Box 9216, Corpus Christi, TX 78469
363. Thomas Zawacki, Manager Appliance Research, Institute of Gas Technology, Energy Development Center, 4201 W. 36th Street, Chicago, IL 60632
364. Floyd J. Zehr, Department of Physics, Westminster College, New Wilmington, PA 16142
365. Congressional Information Service, Research Building 83, Kodak Park, Rochester, NY 14050
366. Edison Electric Institute, 8th Floor, 1111 19th Street, NW, Washington, DC 20036
367. Office of the Assistant Manager for Energy R&D, U.S. Department of Energy, Oak Ridge Operations, Oak Ridge, TN 37831
368. National Energy Information Center, Library, Room 1404, 12th and Pennsylvania Avenues, NW Washington, DC 20461

369–395. Technical Information Center, Department of Energy, P.O. Box 62, Oak Ridge, TN 37831

396–405. External Energy Conservation Distribution, Oak Ridge National Laboratory, Building 9102-2, Conference Room 218, Oak Ridge, TN 37831

☆U.S. GOVERNMENT PRINTING OFFICE: 1986-631-056/20255

ORNL/CON-173 HEAT PUMP WATER HEATER LABORATORY TEST AND DESIGN MODEL VALIDATION